Squeeze casting as alternative fabrication process for carbon fiber reinforced aluminium matrix composites

by

Muhammad Faisal Alam

A thesis submitted to the Faculty of Graduate and Postdoctoral Studies
in partial fulfillment of the requirements for the degree of

Master of Applied Science
in
Mechanical Engineering

Ottawa-Carleton Institute for Mechanical and Aerospace Engineering
University of Ottawa
Ottawa, Canada
April 2013

ABSTRACT

Aluminium matrix composites are among the most promising candidate materials for light weight and high strength applications such as transportation and armour. In a previous study 6061 aluminum matrix composites reinforced with plain weave carbon fiber preform (AS4 Hexcel) were successfully fabricated by squeeze casting using the laminate fabrication technique. This research aims at optimizing the fabrication process in order to achieve improved strength and mechanical properties. It focuses on the liquid infiltration squeeze casting method. Good mechanical bonding between fiber and aluminium is achieved thanks to improved infiltration and impregnation of the fabric by liquid aluminium. Oxidation products at fiber/aluminium interface and porosity are reduced. As a result, composites are produced with overall improved mechanical properties. The flexural strength is increased by up to 19.9% and 15.4% compared to the laminate approach and the reference 6061 aluminium alloy squeeze cast under identical conditions, respectively. Similarly, overall hardness is improved. However, the impact strength is reduced by 7.76% and 25.78% when compared to casts fabricated by the laminate method and the reference aluminium alloy, respectively. The thesis constitutes a good basis for further research on fiber and particle reinforced aluminium matrix composites with the goal of further improving fracture toughness, particularly for gradient materials used in armour applications.

ACKNOWLEDGEMENTS

I am thankful to my God who blessed me with all the abilities necessary to accomplish all my goals. It is my great pleasure and experience working with my professor Michel Nganbe. I would like to express my sincere gratitude to my supervisor for extending his endless efforts, inspiration and guidance throughout this project. I also would like to thank the Faculty of Graduate and Post-Doctoral Studies (FGPS), Professors and all the staff of the Mechanical Engineering Department at the University of Ottawa for providing all kinds of support and a better working environment. I would like to thank my brother and sisters for great love and support. Finally, my deep gratitude goes to my parents and grandparents for their love and prayers; to my wife and little daughter for their patience and for sacrificing enough time to enable me to become more efficient towards my studies.

TABLE OF CONTENTS

LIST OF TABLES

LIST OF FIGURES

NOMENCLATURE

MMCs	Metal matrix composites
AMCs	Aluminium matrix composites
PAN	Polyacrylonitrile
CTE	Coefficient of thermal expansion
OM	Optical microscopy
SEM	Scanning electron microscopy
EDX	Energy-dispersive X-ray spectroscopy
HV	Vickers hardness
σ	Flexural stress
E	Flexural modulus
ε	Flexural strain
ρ	Density
V	Volume fraction
σ_f	Fiber flexural strength
σ_m	Matrix flexural strength
σ_c	Composite flexural strength
E_c	Elastic modulus of composite
E_f	Elastic modulus of fiber
E_m	Elastic modulus of matrix
M	Moment about the neutral axis

I	Area moment of inertia
C	Perpendicular resistance to the neutral axis
P	Midspan load
D	Maximum deflection of the center of the beam
m	Slope of the initial elastic section of the load-deflection curve
b	Width of specimen
d	Thickness of specimen
L	Length of specimen
E_{abs}	Energy absorbed during impact
v	Seepage velocity
k	Permeability
μ	Viscosity

Subscripts:

c	composite
m	matrix
f	Fiber

1 MOTIVATION AND INTRODUCTION

1.1 Motivation

During the past quarter-century, specific material property requirements for advanced applications have tremendously increased, making many conventional alloy systems inappropriate. Therefore, composites have emerged as a class of materials providing enhanced mechanical, physical and thermal properties. Their performance is being optimized making them increasingly superior to their monolithic material counterparts [1]. The fibers provide strength and stiffness to the material, and the matrix holds the fibers in place and transfers internal loads between them. The matrix also protects the fibers from environmental damage [2]. Composites are engineered materials whose properties are directionally specific and can be tailored according to specific application requirements [3] [4].

The applications of metal matrix composites (MMCs) range from military and commercial aircraft to helicopters and spacecraft, automotive and marine [5], electronics, sports industries, and electrodes for metal plating processes. Particularly, for high temperature applications, polymer matrix composites are inappropriate due to their low melting point. Therefore, either metals, MMCs or in the case of extreme temperatures, ceramic matrix composites must be considered [6]. Currently, both Airbus (A350) and Boeing (787) are developing next-generation aircrafts with over 50% composites [3].

Metal matrix composites are widely used in aviation industry which includes turbofan engine blades [7]; blades-engine connections for the Eurocopter; lower drag brace for the F16 main landing gear [8]; struts of US space shuttle fuselage [9]. MMCs are also interesting for space structure applications due to their excellent specific mechanical properties, high thermal

and electrical conductivity, and low coefficient of thermal expansion. In particular, graphite reinforced aluminium composites are often desirable as they offer almost zero coefficient of thermal expansion.

Composite materials, especially those made of carbon fiber, have better specific properties than many traditional materials. The maximization of the strength/weight ratio is desirable, especially for industries driven by weight reduction such as transportation and wind-energy [3]. Application examples include Honda engine blocks with MMC cylinder liners; Toyota diesel engine piston; disk brakes for aircraft and racing cars [9]; drive shafts, brake rotors and calipers in the automotive and railway industries. The demonstrated reduction in overall engine weight varies from 15 kg to 35 kg [1]. Squeeze cast aluminium matrix composite pistons are widely used in heavy-duty diesel engines. The low coefficient of thermal expansion of composites enables near "zero" clearance pistons by reducing piston clearance from 0.051 mm to 0.005 mm which minimizes ring seal leakage [1]. The dimensional stability of MMCs makes them appropriate for tools and dies for shape metal parts [6]. The extremely high stiffness of graphite fibers enables composites to meet space structure application requirements such as in antennae and telescopes where precise pointing and tracking are required [6].

1.2 Introduction

Metal matrix composites can potentially offer many advantages over metals and their alloys. Major advantages include higher specific mechanical properties like modulus-to-density and strength-to-density ratios; improved fatigue life [10]; higher application temperature because of the stable second phase that is contained in the metal matrix [6] [11]; as well as good wear resistance and low thermal expansion [12]. When compared to polymer matrix

composites, metal matrix composites have potential benefits such as good electrical and thermal conductivity; no moisture absorption; no out-gassing in vacuum; metallic joining concepts may be more directly usable; higher temperature utilization; and less degradation of properties [6].

Although many MMCs are attractive for use in different industrial applications, aluminium matrix composites (AMCs) have proved most attractive particularly thanks to their exceptional stiffness-to-weight and strength-to-weight ratios. In addition AMCs show enhanced directional properties; great retention of properties at elevated temperature; fatigue, creep [13] [14] and wear resistance [12] [15]; as well as good durability, machinability, availability, effectiveness and low cost [16] [17] [18].

Of all fabrication methods such as rheocasting, compocasting and powder metallurgy [19] [20], the squeeze casting method is the most developed and advantageous technique for commercial applications. The major advantages of squeeze casting include: (1) elimination of porosity and shrinkage with good dimensional accuracy and surface finish in the casting [5]; (2) capability of production at large scale; (3) well-known technical conditions; (4) improvements in the wettability at interfaces [16]; (5) solidification under pressure producing near zero defects with better metallurgical properties [16] [21]; (6) ability to limit reinforcement at only selected regions of parts [16]. Pressure on the solidifying liquid produces virtually near net shape and fully dense castings [21].

The present work deals with the fabrication of Aluminium Matrix Composites (AMCs) by squeeze casting technique. Carbon fiber fabric preform (AS4 Hexcel) and 6061 alloy matrix are used. Mechanical properties such as hardness, impact strength and bending resistance are studied. The properties thus obtained are compared with those of reference squeeze cast

aluminium fabricated under identical conditions as well as composites fabricated in a previous study using a laminate approach.

Characterization of the castings is done using optical and scanning electron microscopes in order to have a good understanding of the relationships between chemical composition, fabrication method and properties.

2 LITERATURE REVIEW

2.1 Properties of aluminium matrix composites

Metal matrix composites are engineered materials with a combination of two or more dissimilar materials (at least one of which is a metal and the other a non-metal) to obtain enhanced and tailored properties [20] [22]. Composites work by integrating high strength, high modulus reinforcements such as fibers in a ductile matrix [4] [6] [23]. Mechanical properties of composites are intermediate between those of the matrix alloy and those of the reinforcement. Fibers take the load (tension/compression) and provide the strength and stiffness to the material while the matrix transfers stresses to the fibers, gives shape to part and protects the fibers from environment damage [2].

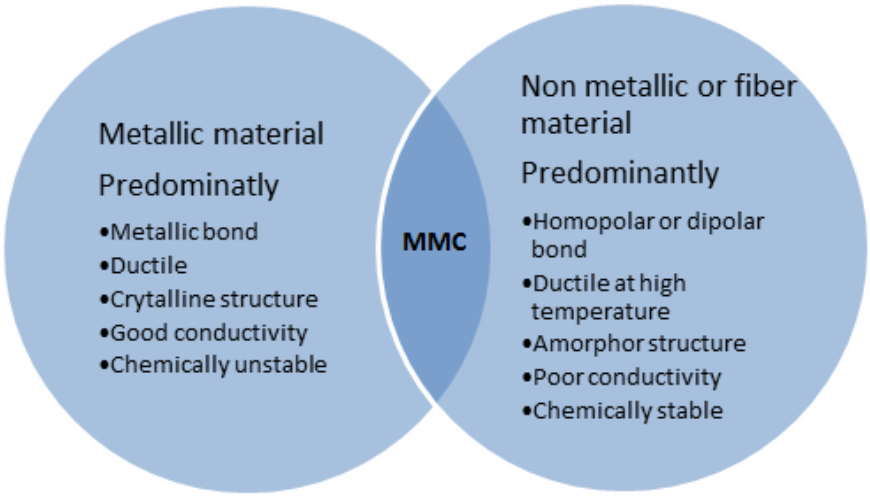

Figure 2-1: Properties of metal matrix composites.

In most composites, fibers such as glass, graphite, boron, pure silica or many whisker crystals are embedded in a matrix yielding high strength and stiffness as well as resistance to crack propagation due to strong interaction between fibers and matrix. Continuous reinforcement composites are characterized by high mechanical strength along the direction of

reinforcement, so they are highly anisotropic. They incorporate better wear resistance, lower coefficient of thermal expansion and higher thermal conductivity in the selected matrix [8]. On the other hand, discontinuous reinforcement composites are almost isotropic [2] [18]. The main combinations of MMC systems can be summarized as in Table 2-1.

Table 2-1: Main combinations of MMC systems [8] [13] [24] [25] [26].

Metal Matrix	Reinforcement Type	Reinforcement Material
Aluminium	Long fiber	Carbon, Boron, Silicon carbide, Alumina
	Short fiber	Alumina, Alumina-silicon
	Whiskers	Silicon carbide
	Particle	Silicon carbide, Boron carbide
Magnesium	Long fiber	Alumina, Graphite
	Whiskers	Silicon carbide
	Particle	Silicon carbide, Boron carbide
Titanium	Long fiber	Silicon carbide
	Particle	Titanium
Copper	Long fiber	Silicon carbide, Carbon
	Particle	Titanium carbide, Silicon carbide, Boron carbide

This work focuses on aluminium metal matrix composites (AMCs). AMCs have usually low density and light weight, high temperature strength, high hardness, high stiffness, high fatigue strength and high wear resistance in comparison to monolithic aluminium [27] [22].

2.1.1 Density

One of the simplest and important physical properties of composite materials is density (ρ). AMCs density can be estimated using the rule of mixture as:

$$\rho_c = \rho_f V_f + \rho_m V_m \text{ [2]} \quad (1)$$

where ρ_c, ρ_f and ρ_m are the densities of composite, fiber and matrix respectively. V_f and V_m $\left(\text{where } V_m = 1 - V_f\right)$ are the fiber and matrix volume fractions respectively.

Thus, the density of a composite can be estimated by the density and the volume fractions of both fiber and matrix [28].

2.1.2 Stiffness and strength / composite micromechanics

Composite micromechanics is the determination of equivalent elastic modulus and strength of a composite material in terms of the elastic moduli and strengths of their constituents [29]. The physical properties of the components or constituents in composites may alter substantially due to phase changes or chemical reactions during fabrication. Excessive difference in shrinkage between the constituents can result in high internal stresses which may lead to premature failure of the composite [30] [31]. Using the rule of mixture, the elastic modulus of MMCs can be given as:

$$E_c = E_f V_f + E_m V_m \text{ [2] [29]} \quad (2)$$

where E_c, E_f and E_m are the elastic moduli of composite, fiber and matrix respectively. It is clear from the above considerations that the addition of fibers with high stiffness can increase the stiffness of the aluminium matrix composite substantially.

2.1.3 Hardness

Hardness is a measure of a material's resistance to permanent deformation or damage caused by a harder material [32]. Hardness tests are generally used as a simple, quick and effective means for assessing the overall mechanical strength of the composite [33]. Most indentation type hardness testing methods are non-destructive [34].

Hardness measurements are useful in determining the suitability of composite materials for a specific application, testing the uniformity of a product, or determining the quality that has been achieved through a manufacturing method. It helps to assess other fundamental properties such as ultimate tensile strength (UTS), yield strength, ductility, compressive strength, toughness and impact strength [34] [35] [36].

Hardness testing is the evaluation of choice for materials under development that can only be produced in small quantities. Consequently, tensile testing requiring relatively large samples are inappropriate and only second choice after hardness testing. There is a proportional relationship between hardness, yield strength and tensile strength as can be seen in Figure 2-2 (a). The same proportionality applies to composites as illustrated in Figure 2-2 (b). For carbon and alloy steels it can be given as:

$$HV \approx 3\,\sigma_{UTS} \quad [34] \tag{3}$$

And for copper and copper-zinc alloys, as:

$$3\sigma_Y < HV < 3\sigma_{UTS} \quad [34] \tag{4}$$

where σ_Y, σ_{UTS} and HV are the yield strength, ultimate tensile strength and Vickers hardness of the material respectively.

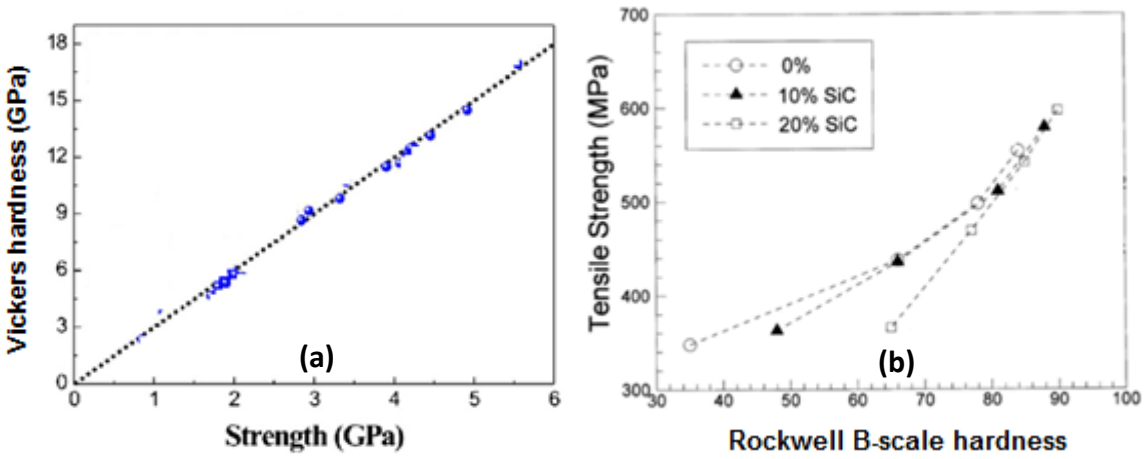

Figure 2-2: Relationship between hardness (Vickers/Rockwell B-scale) and strength for (a) carbon and alloy steels [34]; and (b) AMCs [33].

The Rockwell indenter is generally a diamond cone with a blended spherical tip of 0.2mm radius or a steel ball indenter. The steel ball indenter is normally 1.588mm in diameter; however, larger diameters may be used for soft materials. Among the several hardness scales, the C scale is the most commonly used. For the B scale, a 100 kg load with a 1.588 mm diameter steel ball indenter is used. For the C scale, a 150 kg load and a 120° conical indenter are used. The Rockwell scales give identical macro-hardness values which do not vary for a given material. The hardness values correspond to the resistance of the material to indenter penetrations and can be given as:

$$\text{Rockwell hardness C} = 130 - \frac{\text{depth of penetration (mm)}}{0.002} \text{ [37]} \qquad (5)$$

where 0.002 mm is a unit division at Rockwell scale.

Equation 5 shows that the hardness is directly proportional to the depth of penetration which in turn is proportional to the indentation diameter. In other words, larger indentation diameters mean low resistance to penetration, and therefore low hardness. The relation between hardness and indentation diagonal is also illustrated in Figure 2-3 for the case of Vickers hardness.

In the Vickers micro-hardness test, a diamond indenter, of square pyramid shape with an angle of 136° between the opposite faces, is pressed into the polished surface of the composite specimen using a standard load as shown in Figure 2-4. Standard loads are 5, 10, 20, 30, 50, 100, and 120 kgf depending on the type of material. The load is maintained for the duration of 10 to 15 seconds. After the load is removed, the length of the indentation diagonals d_1 and d_2 are measured with an optical microscope. The Vickers hardness number Hv is defined as the applied load (F) divided by the area of the indent on the specimen and is given by:

$$Hv = \frac{2F}{d^2}\sin\frac{136^o}{2} = 1.854\frac{F}{d^2} \text{ [37]} \quad (6)$$

where the mean diagonal is d =(d_1 + d_2)/2 in mm; F is load in kgf.

Again, Equation 6 shows the inversely proportional relationship between hardness and indentation size.

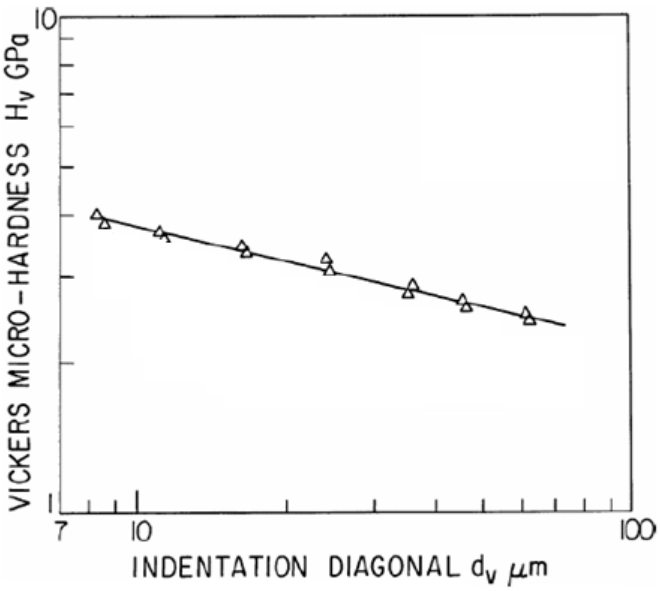

Figure 2-3: Relation between hardness and indentation diagonal [37].

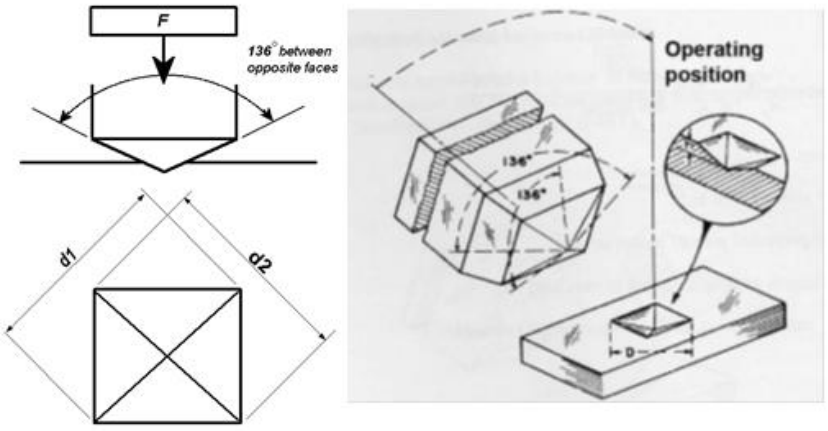

Figure 2-4: Sample indentation during Vickers hardness testing and illustration of the indentation diagonals [38].

2.1.4 Thermal expansion, thermal and electrical conductivity

The thermal expansion coefficient of AMCs reinforced with carbon fiber is much lower compared to that of polymer matrix composites. The electrical conductivity of aluminium is higher than that of carbon fiber. Therefore, Al-composites with high carbon fiber volume fraction show low electrical conductivity. As carbon fibers have very low coefficient of thermal expansion, increasing their volume fraction can yield composites with coefficients of thermal expansion at the level of steel [39]. The electrical conductivity of composites can also be described by the rule of mixture and is influenced by the application temperature [10].

2.1.5 Toughness and failure

When a material is deformed by external loading, it absorbs and stores strain energy throughout its volume. It is sometimes referred to as internal work. The strain energy recovered during unloading is called the Elastic Strain Energy, and the energy which is lost in the process of permanently deforming the material is called Inelastic or Plastic Strain Energy. The strain energy per unit volume of the material is known as Strain Energy Density. The toughness is a measure of the energy per unit volume that can be absorbed by a material without breaking and

is important in resistance to crack and crack propagation [28]. Whereas strong materials have high ultimate stress, a tough material has large area under the stress-strain curve, and therefore requires more energy to get fractured, as seen in Figure 2-5.

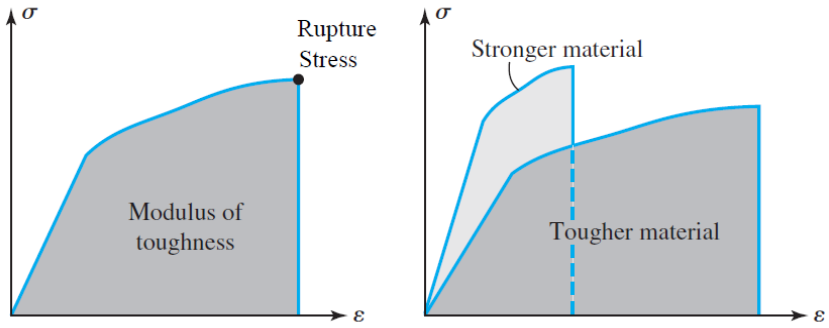

Figure 2-5: Energy related moduli [40].

The bulk failure of metal matrix composites can result from either:

- Ductile failure by nucleation, growth, and coalescence of cracks in the matrix [dominant failure process in many fiber reinforced Aluminium Matrix Composites (AMCs) and particle reinforced AMCs]
- Or brittle failure of the reinforcement

The low ductility or brittleness of MMCs causes crack initiation that generally begins at interfaces. Therefore, the overall mechanical performance and the failure mechanism of composite materials not only depend on bulk properties, but also on interface properties or possible fracture along the interface between the matrix and the reinforcement [1].

The ability of a material to remain serviceable when containing cracks, or when cracks develop during service, depends upon its toughness. The failure mode of fibers in the composite mainly depends on the adhesion between fiber and matrix. With low adhesion, the filaments delaminate from the matrix, and the fibers undergo columnar buckling. At intermediate adhesion strength, the fibers undergo micro-buckling along the line of maximum

shear stress. And at high adhesion, fiber compressive failure occurs in several planes due to strong fiber/matrix adhesion. Therefore, the fibers can be compressively loaded to their maximum capacity [14].

Composite failure mechanism and mode are influenced by the following factors [1]:

- The size, shape, concentration and distribution of the reinforcement.
- The concentration of impurities present in the constituent phases of the composites.
- The production method and heat treatment processes, including any aging treatments, to which the composite is subjected prior to mechanical loading.
- The coatings applied to the reinforcement (if any).

Composite materials are inherently heterogeneous in nature, causing undesirable effects at interfaces because of [1]:

- Reinforcement clustering.
- Larger volume fractions of reinforcements.
- Larger particles (greater probability of finding a pre-existing crack or the probability of the occurrence of a larger size flaw within the particle which can cause premature particle fracture). Large size foreign particles provide the primary nucleation sites for the formation of cavities in composites. However, the growth of large cavities can be facilitated by voids formed around smaller particles that can then coalesce by the linkage of cavities nucleated around dispersoid particles and fibers [1].

These imperfections at interfaces support nucleation of cavities and cracks. Furthermore, the sharp corners of the reinforcements exhibit geometric imperfections that can promote damage initiation and growth [1]. In the case of composites showing a very strong fiber/matrix

interface, the fibers are likely to break along the matrix crack. This is the case even if matrix fracture occurs by a ductile mechanism as shown in Figure 2-6 (a). If the matrix is weakly bonded, the stress concentration field at the matrix crack tip causes debonding that leads to fiber pull-out to achieve full crack surface separation. This is shown in Figure 2-6 (b).

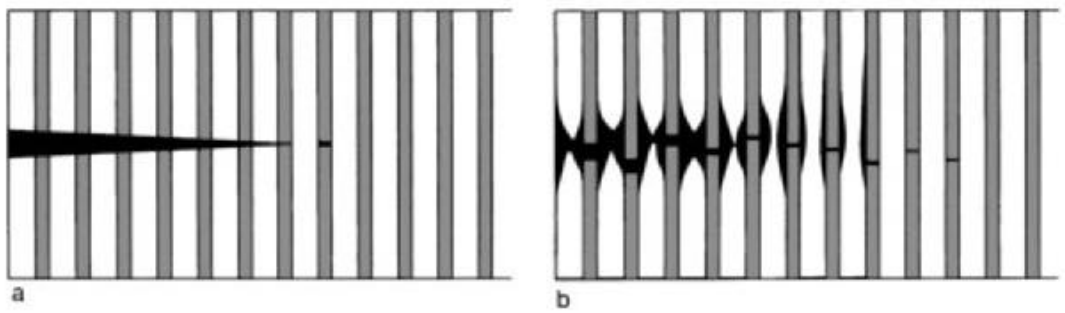

Figure 2-6: Crack propagating through long fiber reinforced MMCs: (a) strong fiber/matrix interface, a planar crack occurs with brittle fracture in the matrix; (b) weak fiber/matrix interface, ductile flow in the matrix leads to fiber/matrix decohesion and nonplanar fracture [1].

The matrix volume that undergoes deformation during fracture is proportional to the fracture toughness and strongly depends on fiber spacing, fiber volume fraction and fiber size [1].

2.2 The fiber/matrix interface

The fiber/matrix bond plays an important role in the load transmission from the matrix to the fibers. Since the fiber is stiffer than the aluminium matrix, it is the fiber that takes most of the applied load. The load at the interface is a shear stress. Therefore, it is essential that the interface be capable of sustaining shear load without failure [1]. Figure 2-7 shows the matrix deformation pattern around the reinforcement fibers. If the fiber/matrix interface shall fail to transmit the load, then fibers may instead weaken the composite due to the volume occupied by such ineffective fibers [17]. Consequently, the plastic deformation of MMCs mainly depends upon the fiber/matrix interface [11].

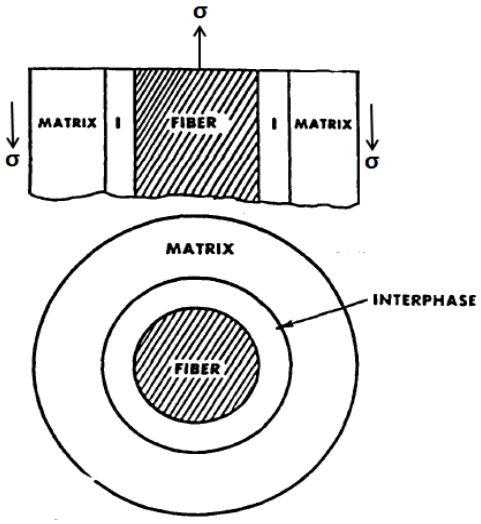

Figure 2-7: Schematic illustration of reinforced composites: the matrix surrounding a fiber that is subjected to tensile load [41].

In fact, the fabrication conditions to which reinforcement and matrix are subjected can produce compounds and/or phases along the fiber/matrix interface that can significantly influence the mechanical properties of the MMCs [8]. This interface or fiber/matrix bond can be classified into three types: chemical diffusion bond, chemical reaction bond and mechanical bond.

The interface layer can result in good adhesion provided that defects such as voids are not produced at the interface. This interface layer is produced by carbon dissolution into liquid aluminium and by diffusion of aluminium atoms into the carbon fibers [8] [42].

The reinforcement/matrix interface bond in MMCs can be a reaction bond taking the form of a layer of reaction products at the interface such as different carbides produced between light alloys and carbon fibers. These reaction products are generally brittle in nature and can be preferential sites for cracks to initiate. These cracks can propagate and eventually cause the composite to fracture [8] [43].

The fiber/matrix bond due to interlocking is created by wetting of the reinforcements or external bond agents. Coating of the fiber with wettable metal or external bond agents (sizing)

such as copper, zinc, magnesium [42] or nickel [15] [44] serves two purposes: it results in better wetting of the fiber by the molten aluminium and restricts chemical reactions at the fiber/matrix interface [44] [45]. Hence, they influence mechanical properties within the fiber-sizing-matrix region. The interface between fiber and matrix is a continuous change from the core properties of the fiber to the core properties of the matrix. The chemistry and mechanical properties at and near the surface may be altered by substantial adsorption of the aluminium matrix and the fiber [14].

During bonding of two dissimilar materials, chemical processes can occur that lead to a modification of the properties of the interface. Therefore, it is essential to also study the chemistry at the interface. If two different materials are brought into close contact, interaction processes may occur that reduce the total energy of the system. This amount of energy is also referred to as work of adhesion, which is the energy required for separating the fiber from the liquid aluminium at the interfaces [14].

Generally, material failure is governed by a main crack nucleating from defects inside the matrix or at the interface between the matrix and the reinforcement. Furthermore, the crack propagation or its arrest strongly depends on the degree of resistance offered by the reinforcement. Obviously, fibers offer strong resistance to crack propagation than the matrix as illustrated in Figure 2-8.

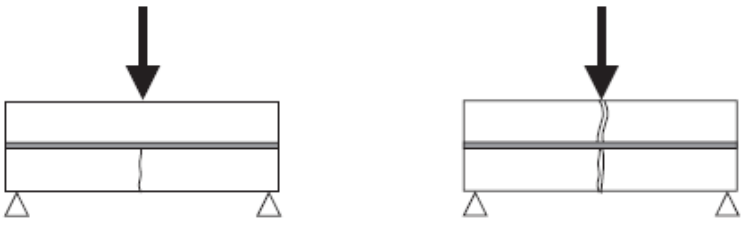

Figure 2-8: Crack propagation through fiber in composites [46].

2.3 Manufacturing of metal matrix composites

Metal matrix composite materials can be produced by many different techniques. By altering the manufacturing method, the type and form of the reinforcements, it is possible to obtain different mechanical properties [26] [27].

MMCs are produced by combining ingredient materials either by casting (molten metal and fiber preforms) or powder metallurgy (powdered metal and loose ceramic particles) methods depending on the type of hardening particles and intended application conditions [19]. Secondary processing follows primary processing, and its aim is to alter the shape or microstructure of the material. Secondary processing includes shape casting, forging, extrusion, heat-treatment, machining [8] [47]. These secondary processing methods can also be used to reduce porosity [44].

This thesis focuses on squeeze casting of aluminium based composites reinforced with woven carbon fiber fabric. The method of pressure infiltration to manufacture composites offers many advantages such as locally reinforced composites with near net shape, good surface quality, high production rate, low production costs, as well as short contact time of liquid metal with reinforcement that considerably prevents degradation of the composites [12] [48]. The liquid metallurgy technique is the most economical of all available techniques in the production of MMCs [27] as it facilitates the flow to fill the interstices and cover the fibers properly [8].

Squeeze casting is a unidirectional pressure infiltration technique especially used for the fabrication of aluminium matrix composites [8]. It combines the advantages of traditional high pressure die casting, gravity permanent mold die casting and common forging technology [5] [19] [49]. It involves the solidification of molten metal under high pressure to eliminate

casting defects [47]. Pressure during solidification helps to achieve near zero defects with improved metallurgical properties [50] [51].

At elevated temperature, carbon fibers react with the molten aluminium alloy to form reaction products. To avoid chemical reactions at fiber/matrix interfaces, fiber surface coating is added which increases the cost [14]. Fibers may be coated to improve wettability of graphite by liquid aluminium as discussed in 2.2. This surface treatment can be avoided in squeeze infiltration method thanks to short liquid-fiber contact time [14]. Besides thorough infiltration, the application of high pressure raises the solidification temperature of the matrix and increases the rate of heat dissipation through the die. This effect minimizes fiber-matrix reaction at the interface and eliminates defects such as gas porosity and shrinkage [45]. Due to high heat dissipation through the die, composites with fine grain structure are obtained [5].

The main cause of porosity in reinforced MMCs is gas entrapment, and the presence of water vapour on the reinforcement surfaces. At temperatures above the liquidus temperature of the aluminium alloy (650–750°C), the solubility of hydrogen gas in molten aluminium is high. However, the gas solubility decreases as the temperature drops. Therefore, when aluminium solidifies, the hydrogen dissolved in molten aluminium alloy gets trapped, which produces gas porosity [52].

The main process parameters in squeeze casting process include [5] [8] [45]:

- infiltration speed (mainly caused by applied pressure)
- spacing between particles of the reinforcement
- duration of pressure application
- die and preform preheat temperature
- molten metal temperature, volume, and viscosity

3 METHODOLOGY

3.1 Materials description

3.1.1 Aluminium

In this study commercially available aluminium alloy 6061 is used as composite matrix. Aluminium is one of the most abundant metals and valuable because of many properties such as its lightweight, high strength, long life, high ductility, machinability, excellent thermal and electrical conductivity, recyclability and corrosion resistance [53] [54] [55]. Some important properties and the chemical composition of 6061 T6 are tabulated in Table 3-1 and Table 3-2 respectively.

Table 3-1: Some important properties of Aluminium 6061-T6 [56].

Physical Properties	**Values**
Density	2.7 g/cc
Brinell hardness	95
Ultimate tensile strength	310 MPa
Yield tensile strength	276 MPa
Modulus of elasticity	69.0 GPa
Linear coefficient of thermal expansion	23.6 µm/m-°C
Thermal conductivity	167 W/m-K
Melting point	582 - 652 °C
Solidus	582 °C
Liquidus	652 °C

Table 3-2: Composition of the matrix alloy Aluminium 6061-T6 [25] [56].

Elements	Wt. %
Magnesium, Mg	0.8 – 1.2
Silicon, Si	0.4 – 0.8
Copper, Cu	0.15 – 0.4
Iron, Fe	0.7 Max.
Manganese, Mn	0.15 Max.
Titanium, Ti	0.15 Max
Zinc, Zn	0.25 Max
Other	0.05 Max
Aluminium, Al	Balance (95.8 - 98.6)

3.1.2 Plain weave carbon fiber fabric

This work focuses on plain weave carbon fibers as composite reinforcement. They are lighter than glass and lower cost [47]. Carbon fibers are perfectly circular in cross-section and usually vary in diameter from 5 µm to 10 µm [57].

A carbon fiber filament is the smallest part of the carbon fiber fabric. Tows or filament bundles are untwisted bundles of individual filaments or strands [58]. A tow can be twisted into a yarn, or several tows combined into a roving. Weaves are the strongest and most stable structures that can be obtained from interlacing yarns.

Plain weave is the simplest weave form that can be produced [59] [60]. The carbon filling or weft yarns (yarn in the 0° direction) and carbon warp yarns (yarn in the 90° direction) are interlaced in a repeated sequence one over and one under pattern. Each warp yarn passes over one pick and under the next; similarly each weft yarn passes over one pick and under the next as shown in Figure 3-1. It provides maximum fabric stability and firmness with minimum

yarn slippage. Different structures and types of woven textiles can be produced depending on required mechanical properties and application conditions.

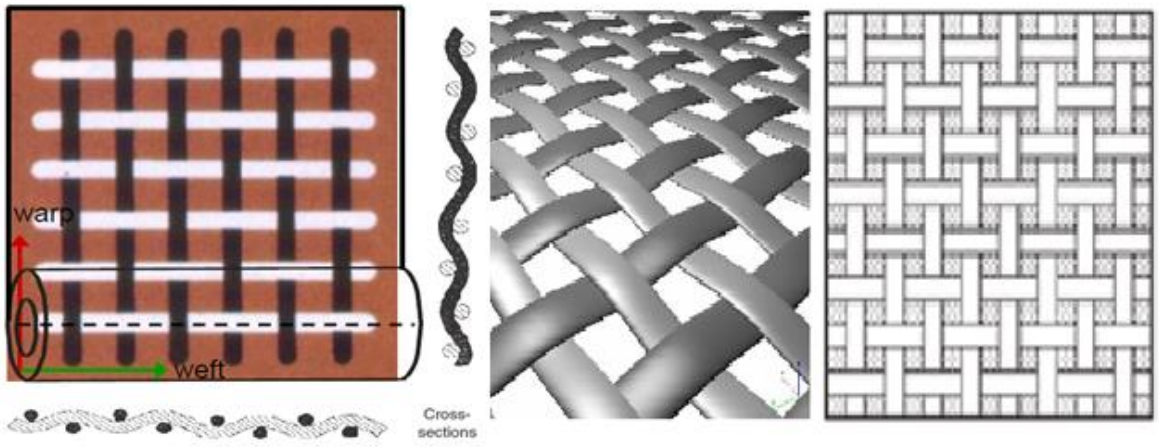

Figure 3-1: Yarn interlacing in plain weave fabric [59] [60] [61].

3.1.2.1 Fibers properties

Carbon fibers have highest specific modulus and offers highest specific strength of all reinforcing fibers; therefore they are used in composites requiring exceptional strength, high stiffness, low weight and outstanding fatigue characteristics in critical requirements [59]. A very important property of carbon fibers is low coefficient of thermal expansion that makes these fibers invaluable in applications where high dimensional stability is required [6]. Carbon fibers also have good electrical conductivity, thermal conductivity, low coefficient of thermal expansion and do not suffer from stress rupture at high temperature as other fibers do [6] [23] [58]**.** Carbon fibers have a hardness of 6.78 GPa which is five times higher than that of aluminium [15]. Similarly, carbon fibers are good for chemical inertness and high damping properties.

AS4 Hexcel Carbon fiber is continuous 3K filament bundles. This is high grade PAN based fiber suitable for high strength and strain applications [62]. AS4 Hexcel fiber is received

as plain weave fabric as shown in Figure 3-2. The properties of the fiber are tabulated in Table 3-3.

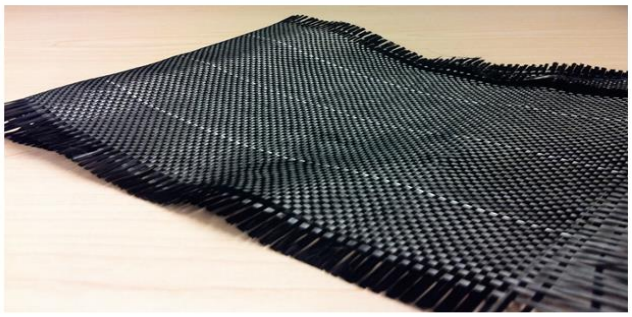

Figure 3-2: AS4 Hexcel plain weave carbon fiber fabric [49].

Table 3-3: Properties of AS4 Hexcel, continuous 3K [62].

Properties	**Values**
Tensile strength	4433 MPa
Tensile modulus	231 GPa
Ultimate elongation at failure	1.8 %
Density	1.79 g/cm^3
Weight/length	0.210 g/m
Approximate yield	4.76 m/g
Tow cross-section area	0.12 mm^2
Filament diameter	7.1 microns
Carbon content	94 %
Specific heat	0.27 Cal/g-°C
Electrical resistivity	1.7 x 10^{-3} Ohm-cm
Coefficient of thermal expansion	0.63 ppm/°C
Thermal conductivity	6.83 W/m-°K

3.2 Manufacturing process

3.2.1 Setup of squeeze casting

For the squeeze casting equipment, stainless steel 316 is selected as it can withstand high temperature and accelerated oxidation environment [63] [64] experienced during squeeze casting.

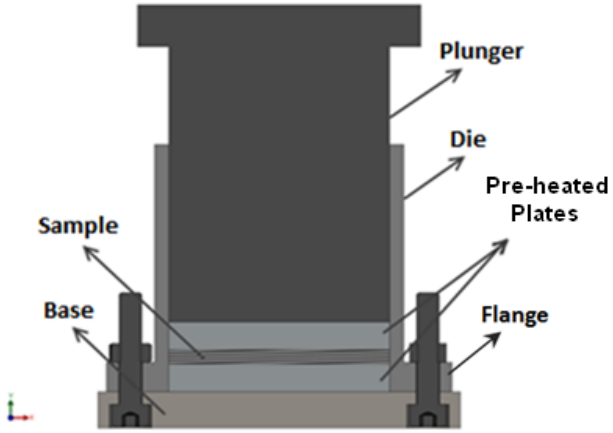

Figure 3-3: Squeeze casting setup [49].

The squeeze casting setup consists of two stainless steel spacers, stainless steel plunger, die, and base as shown in Figure 3-3. The cylindrical die is designed in order to minimize leakage, provide uniform pressure [49], and ensure smooth ejection of the cast [21]. The die cavity has an internal diameter of 78 mm with 5.5 mm wall thickness. It is connected to a 12 mm thick perfectly flat welded flange of 122 mm diameter using head cap screws and nuts. The plunger is a close fit to the die cavity in order to minimize leakage. The plunger is designed to be 50 mm longer than the die depth in order to be also used as ejector of the squeeze cast sample.

High temperature mold release (white graphite) spray is used as lubricant. A thin film of mould release is applied to the inner walls of the die cavity, plunger, base plate and the spacers. The purpose of using the mold release is twofold. First, it prevents adhesion and sticking of the composite specimen to the inner die wall, the steel spacers and to the punch. Second, it facilitates the sample ejection from the die after squeezing.

Excess molten aluminium is poured into the die for each experiment to minimize the effect of temperature drop, when molten aluminium comes in contact with the punch. The additional aluminium provides surplus heat capacity and helps prevent the deterioration of fluidity and impregnation capacity of the molten aluminium.

A 50 mm thick ring is used to support the die during the ejection of the sample after the die base has been removed. Two close fit, 14 mm thick stainless steel spacers were used. One between sample and punch and the other between sample and die base. The spacers are used to maintain pressure and achieve minimum leakage of molten aluminium during squeezing.

3.2.2 Sample manufacture

Extruded aluminium A6061-T6 rods with 50 mm diameter are used. A band saw is used to cut the rods into appropriate sizes. The aluminium charge is molten in a graphite crucible cup placed inside a Lindberg Blue M vertical type furnace as shown in Figure 3-4. Simultaneously the preform is heated in a horizontal type LINDBERG convectional furnace as shown in Figure 3-5. A graphite crucible is selected due to its high thermal shock resistance. It has a molded-in pouring lip to facilitate pouring of molten aluminium into the die cavity as shown in Figure 3-6.

Figure 3-4: Lindberg vertical furnace used to melt aluminium 6061.

Figure 3-5: Lindberg horizontal furnace used to preheat the fiber preform.

Figure 3-6: Graphite crucible cup to handle the molten aluminium alloy.

Carbon fiber density, if required, is reduced by removing alternate yarns using tweezers. In order to maintain the original arrangement of the plain weave fabric and to prevent the movement of the fiber bundles, the carbon fiber fabric is first cut using scissors to a square shape. After appropriately removing fibers and obtaining the required fiber density as shown in Figure 3-7 (a), the square preform is then clammed and pressed between two aluminium plates (template) of the die size and cut to the required shape as shown is Figure 3-7 (b).

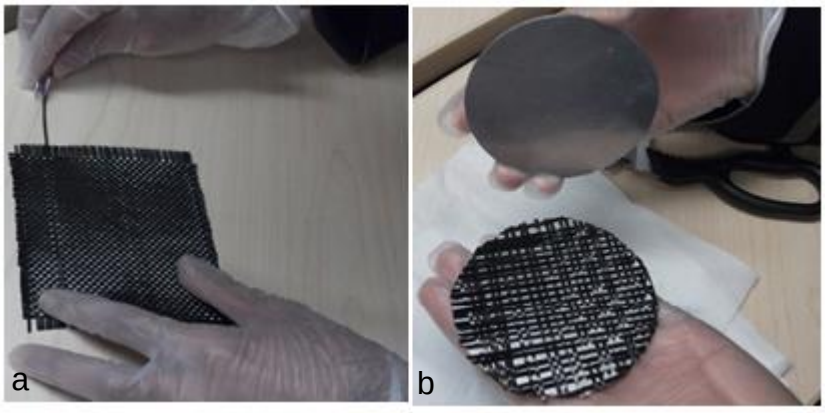

Figure 3-7: Preparing AS4 Hexcel preform by removing alternate yarns of fiber fabric.

3.2.3 Squeeze casting process

The preform (fiber) is placed in the die and pre-heated [5] to 550°C. Heating is required to enhance the wettability with the molten matrix alloy [27] [44] which helps in reducing the

porosity in the final composite [52]. The plunger is also pre-heated separately in the same furnace in order to reduce heat losses and rapid temperature drop as the plunger comes into contact with the molten aluminium charge during squeezing. The heating time from room temperature to 550°C is about an hour. The aluminium 6061 alloy charge is melted and maintained at 850°C (typically between 150–250°C above its liquidus temperature [5]) for about 40 min in order to homogenize its temperature and viscosity.

The die is placed in the squeeze equipment consisting of a 50 ton hydraulic press as shown in Figure 3-8. The molten aluminium is then poured into the die; the plunger inserted into the die from the top; and the pressure is applied while liquid aluminium solidifies [5] [8]. If the melt solidifies prior to infiltration into the preform, perfect infiltration cannot be obtained and severe damage of preform is caused by squeezing in the presence of solidified particles [16] [51]. Therefore, all steps shall go quickly from the time the crucible is taken out from the furnace to pouring the molten aluminium into the die, to pressure application. Constant squeeze pressure is maintained 1 to 2 minutes during which the plunger is further pressed downward in order to compensate for any shrinkage. Relatively low squeeze pressure of approximately 20 MPa is applied to avoid excessive damage of the fiber [16]. The ram of the hydraulic press is disengaged and the screws joining the base plate to the die are released. The plunger is further pressed by again using the ram, until the cast is completely ejected out from the die.

Figure 3-8: Hydraulic press (50 ton) for squeeze casting setup.

The complete squeeze casting process is illustrated in the flow chart in Figure 3-9 below:

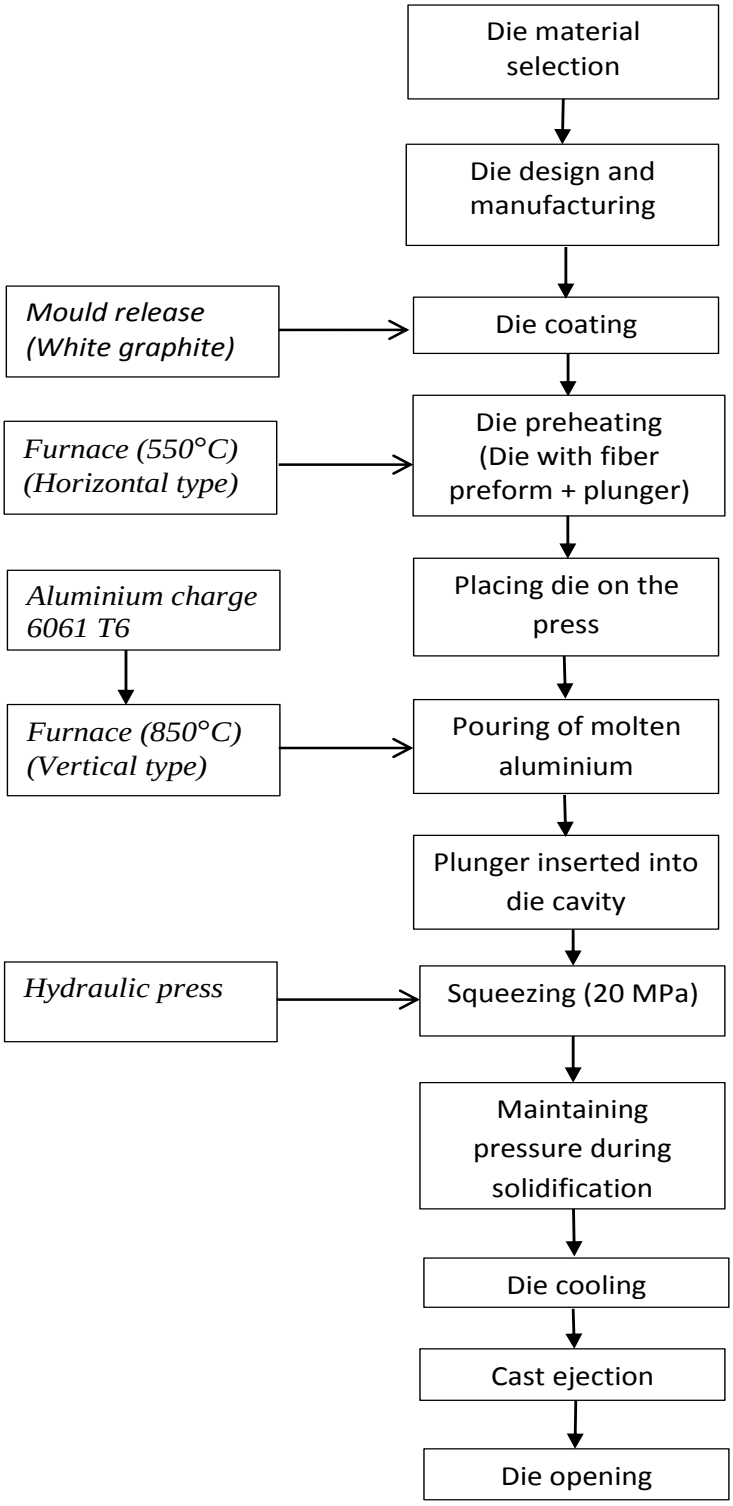

Figure 3-9: Squeeze casting flow chart.

For direct comparison, the liquid infiltration method used in this work is compared to the laminate method developed in a previous study. In the laminate method, aluminium sheets/foils and carbon fiber fabric were alternatively placed in the die as shown in Figure 3-10. The die containing the sample is then heated and maintained at 850°C for about 30 min in the furnace to homogenise the temperature. The plunger was then inserted into the die and the sample was squeezed under a pressure of approximately 20 MPa.

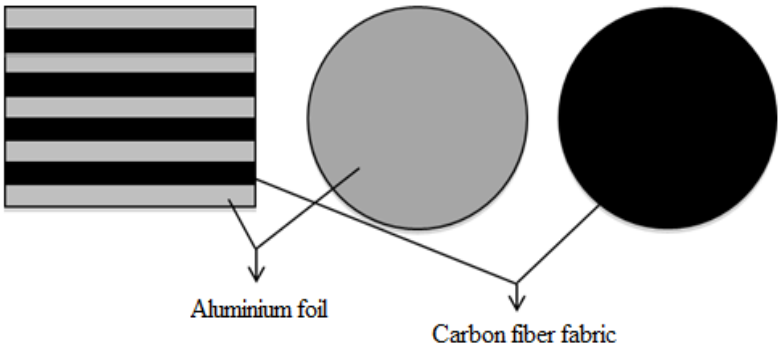

Figure 3-10: Sample preparation in the laminate method [49].

3.3 Mechanical testing

Impact, hardness, and bend tests are conducted. The behaviour of the composite obtained by squeeze casting is compared to that of the reference aluminium alloy casted under identical conditions. The liquid infiltration technique is also compared to the laminate method used in the previous study [49].

3.3.1 Impact testing

The energy absorbed prior to fracture or the resistance of composite beam samples to breakage is determined using Charpy impact test as shown in Figure 3-11.

Figure 3-11: Charpy impact test equipment.

Specimens for the impact test are rectangular bars cut in dimensions of 70 mm length (*L*), 12 mm width (*b*), and 3.64 mm to 6.00 mm thickness (*d*). Notches are not cut in the samples for simplicity. When the swing pendulum strikes the composite specimen, the specimen absorbs energy until yielding. At this point, the specimen starts to undergo plastic deformation. When the sample can no longer absorb more energy, fracture occurs [5].

The sample is held in place at both ends in the test fixture as shown in Figure 3-12. It is hit by the pendulum of the test equipment at the speed of 3.46 m/sec. Toughness and failure mode of each specimen are evaluated by visual examination of the fracture surface [65].

Figure 3-12: Specimen in fixture of the Charpy impact tester.

3.3.2 Hardness testing

Hardness tests are performed at two scales [66]:

(1) Macro hardness is performed using a Rockwell hardness tester (see Figure 3-13). Because of the relatively low hardness of the composites that is out of scale, no hardness values can be determined and only the indentation diameter is used as measure of the composite bulk hardness [67]. The hardness tests are conducted at room temperature with 150 kg indentation load on the thickness surface in order to deform both matrix and fiber layer. An optical microscope is used to measure the indentation diameter as shown in Figure 3-14.

Figure 3-13: Rockwell macro-hardness tester.

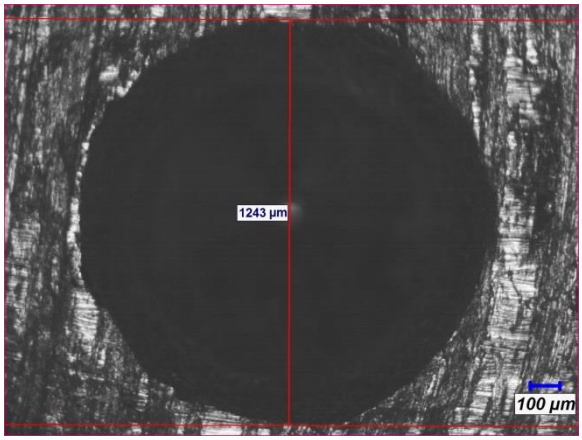

Figure 3-14: Indentation diameter measurement using optical microscope.

(2) Vickers hardness tests are used to investigate the local hardness, the adhesion between the fiber and matrix and the formation of different phases at the fiber/matrix interface. These tests are performed using a STRUERS DURAMIN A/S DK-2750 micro-hardness testing machine (Figure 3-15). An indentation load of 500g (Hv0.5) is used and hardness values are obtained from the digital output of the machine.

Figure 3-15: STRUERS DURAMIN micro-hardness testing machine.

3.3.3 Three point bend test

Three point bend tests are used to measure the force required to bend a beam under 3 point loading conditions. Specimens for the three point bend tests are rectangular bars cut in

dimensions of 55 mm length (L), 12 mm width (b), and 3.64 mm to 6.0 mm thickness (d). A test specimen is held as a simply supported beam and is subjected to three-point bending [68] as shown in Figure 3-16. A computer controlled Instron universal test frame is used as shown in Figure 3-17. The cross-head displacement speed is 10 mm/min and the deflection is measured up to 2 to 5 mm after the start of fracture.

The flexural modulus (E) can be obtained from Hooke's law using Equation:

$$E = \frac{\sigma}{\varepsilon} \text{ [69] [70]} \tag{7}$$

where

$$E = \frac{L^3 m}{4b\, d^3} \tag{8}$$

$$\sigma = \frac{3PL}{2b\, d^2} \tag{9}$$

and

$$\varepsilon = \frac{6Dd}{L^2} \tag{10}$$

where P is the midspan point load (N); D is the maximum deflection of the center of the beam (mm); and m is the slope of the elastic region of the load-deflection curve. Bend tests are only intended for relative comparison between the different investigated samples.

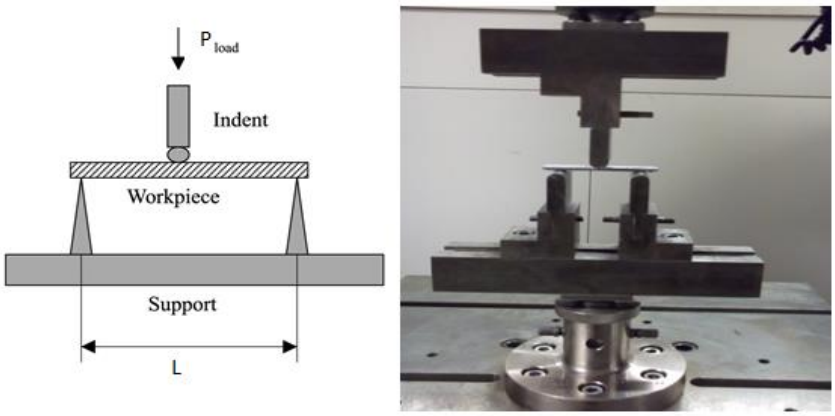

Figure 3-16: Setup for the bend tests.

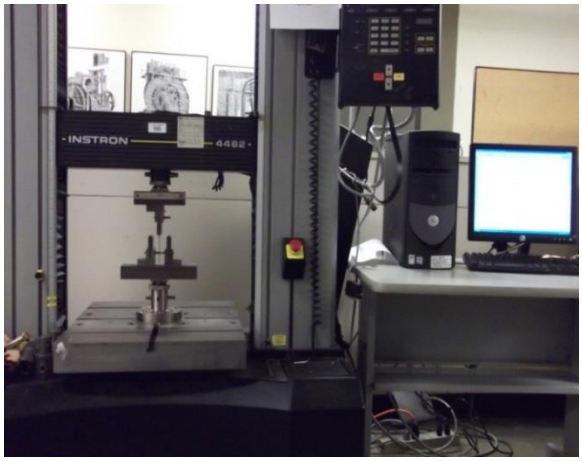

Figure 3-17: Instron universal testing machine for the bend tests.

3.4 Microscopy

Optical and scanning electron microscopy investigations are used for microstructure, chemical composition, phase formation at the interface, and porosity characterization. Metallographic samples are prepared for all cast samples. STRUERS Secotom-10 equipped with a digital controller is used to cut the specimens using a silicon carbide cutting blade. The specimens are then mounted in resin using a STRUERS LaboPress-3 at 20 kN pressure and 150ºC for 12 min. Grinding and polishing are carried out using a STRUERS Tegrapol-31 machine.

Optical microscopy is performed using an XJP-3A microscope (Figure 3-18, left). It is equipped with a Clemex video camera to take and save images to a computer for subsequent image analysis using Clemex vision 4.0. SEM ZEISS EVO-MA10 (Figure 3-18, right) is used for scanning electron microscopy examination. It is equipped with EDX spectrometry detector for chemical analysis and phase investigations.

Figure 3-18: XJP-3A optical microscope (left) and ZEISS electron microscope (right) used for microscopy.

4 RESULTS

Composites reinforced with different carbon fiber volume fractions are investigated as shown in Table 4-1.

Table 4-1: Samples investigated with different fiber densities.

Samples	No. of fiber layers	Type of fabric
S_1	6 fiber layers	Original fiber fabric
S_2	9 fiber layers	Original fiber fabric
S_3	12 fiber layers	Original fiber fabric
S_4	24 fiber layers	Fiber fabric with every second fiber yarn removed
S_5	30 fiber layers	Fiber fabric with every second fiber yarn removed
S_A	6061 (T6) aluminium	Reference alloy (without fiber layers), Fabricated by squeeze casting

4.1 Microstructural evaluation and chemical composition

Microstructural analysis of all the samples was conducted using Optical Microscopy (OM) and Scanning Electron Microscopy (SEM). Optical microscopy is used to investigate the porosity in the cast composites, while scanning electron microscopy is used to characterize the formation of new phases, the fiber/matrix interface, and the chemical composition. This section explains the variation in the microstructure based on the fiber density achieved by varying the fiber spacing. It also compares the results of the infiltration method with those of the reference aluminium and the laminate method.

4.1.1 Optical microscopy analysis

A quantitative porosity assessment at interfaces is done using optical microscopy. The dark gray areas are identified as carbon fiber and the remaining light gray zones as the matrix with virtually zero porosity [8] [71] as seen in Figure 4-1. In contrast, porosity can be seen as dark patches in the composites fabricated by the laminate method as shown in Figure 4-2.

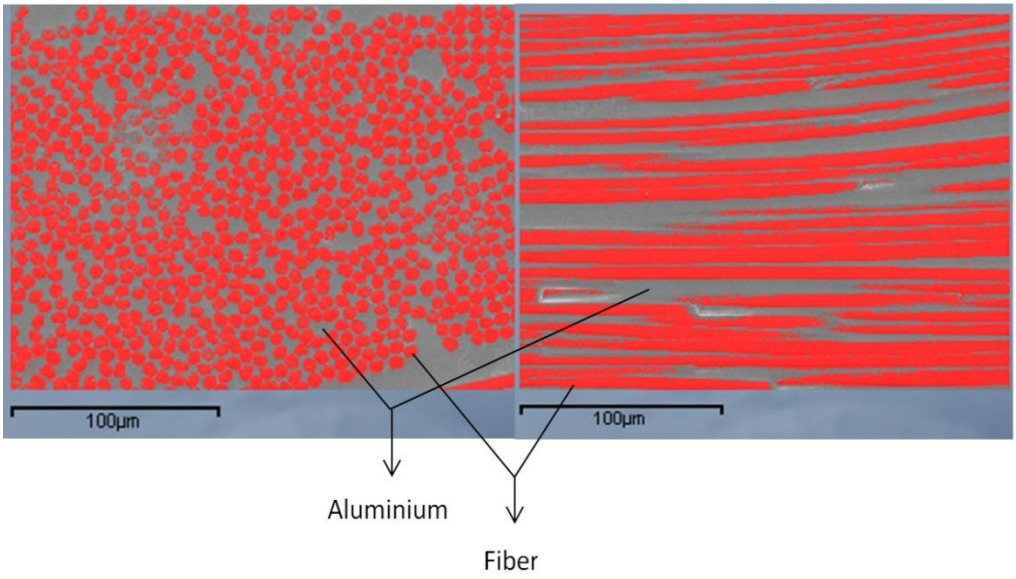

Figure 4-1: Porosity analysis at the carbon fiber/aluminium matrix interface (no porosity observed).

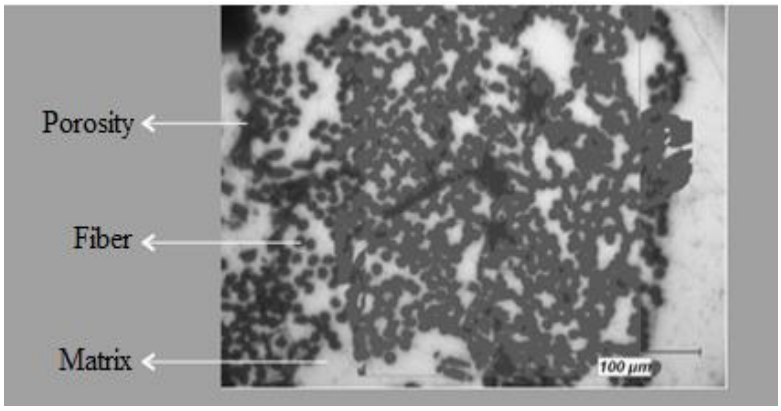

Figure 4-2: Porosity analysis at the carbon fiber/aluminium matrix interface (laminate method). Some porosity can be observed at fiber/matrix interfaces [49].

4.1.2 Scanning electron microscopy analyses

A SEM micrograph of sample S_5 is illustrated in Figure 4-3 and shows the matrix boundary between two orthogonal layers of plain weave. The matrix region of the samples containing the original fiber fabric differs from that of the low density fiber fabric, and the variation in the interspacing between plain weave tows affects the composites' overall properties. A similar fiber fabric configuration was obtained in composites fabricated by the laminate method (see Figure 4-4) except that no porosity was observed in the case of liquid infiltration.

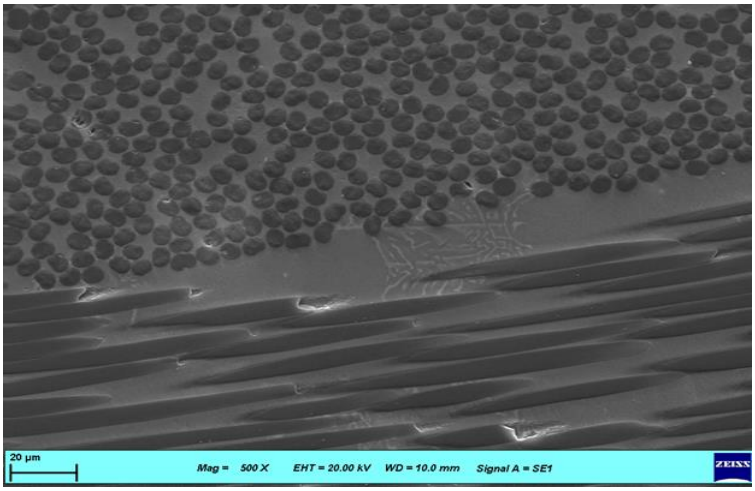

Figure 4-3: SEM micrograph of sample S_5 showing aluminium matrix and carbon fiber layers.

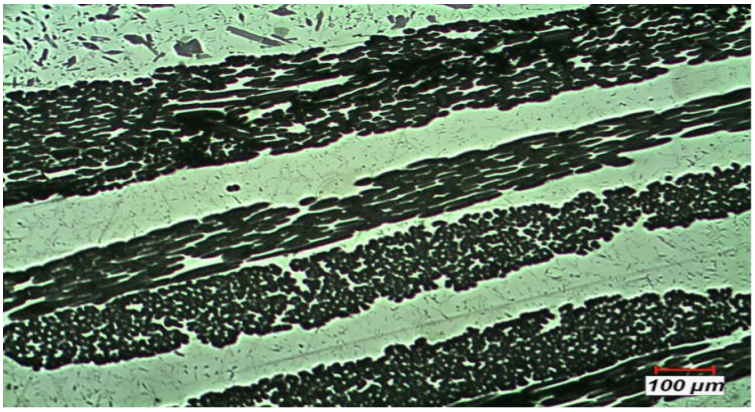

Figure 4-4: SEM micrograph showing aluminium matrix and carbon fiber ply laminates (laminate method) [49].

Due to the lack of interspacing between fiber layers as they are laid in the casting die prior to casting, the liquid infiltration method yields overall higher fiber volume fractions in the composites compared to the laminate method as illustrated in Figure 4-5.

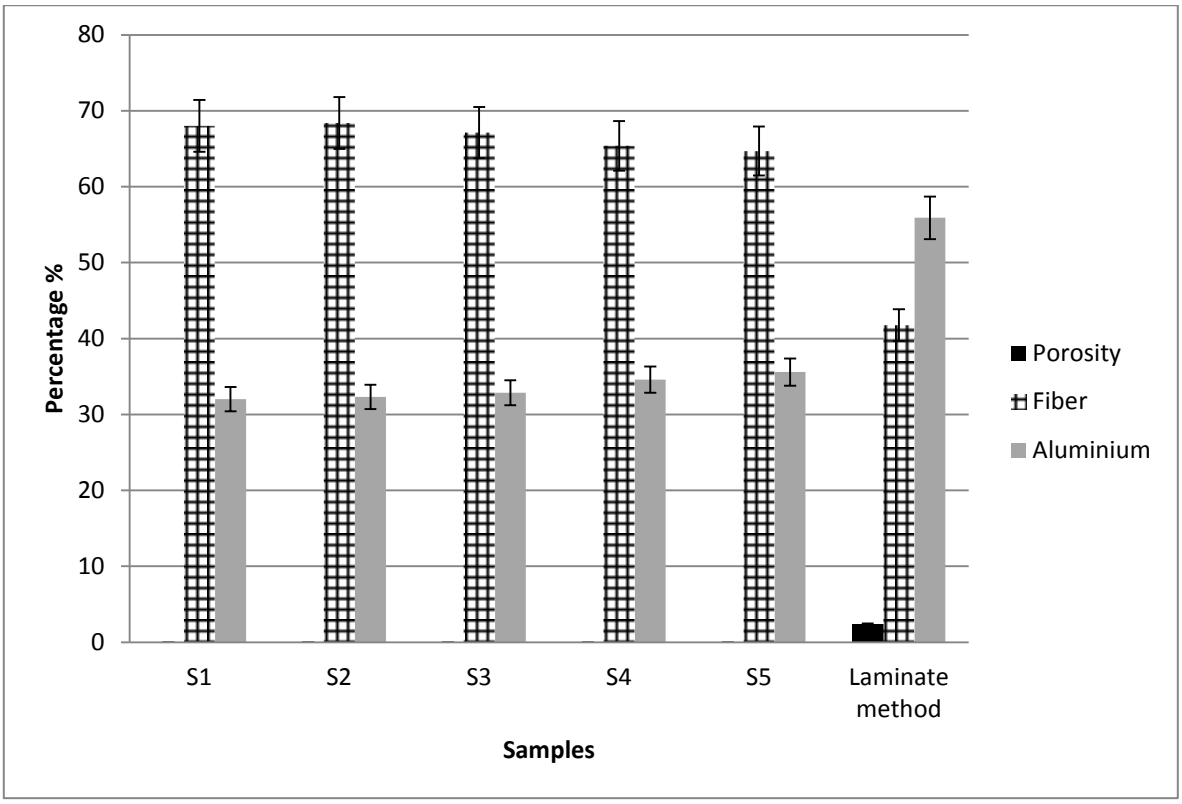

Figure 4-5: Amount of carbon fiber, porosity and aluminium in samples.

4.1.3 EDX analysis using scanning electron microscopy

SEM EDX (Energy-Dispersive X-Ray Spectroscopy) is carried out for chemical analysis. Precipitation of elements is observed at some regions near the interface as shown in Figure 4-6.

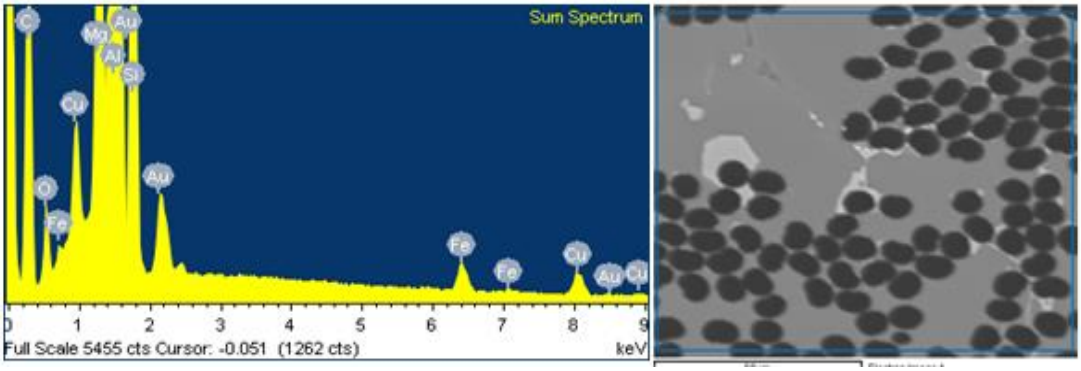

Figure 4-6: SEM EDX area mapping of sample S_5.

Table 4-2: Element contents in sample S_5.

Elements	Al	C	O	Mg	Si	Fe	Cu	Mn	Au	Total
Wt %	27.57	62.77	2.45	1.35	2.91	0.49	0.81	0.38	1.27	100

It is evident from the element contents summarized in Table 4-2 that other than aluminium and carbon, oxygen, magnesium, and silicon are present. Between the different samples, the weight percentages of aluminium and carbon are almost identical. Precipitates are also observed clustered together at grain boundaries within the matrix and at the fiber/matrix interface as can be seen in Figure 4-7. In contrast, precipitates appeared to be lamellar in the case of the laminate method as can be seen in Figure 4-8. The results of EDX analysis are summarized in Table 4-3. The precipitates mainly contain about 8.32wt% iron and 8.78wt% silicon, which is a significantly higher amount than in the aluminium matrix.

Carbon from the fiber diffuses into aluminium leading to a higher concentration of carbon in the matrix. As illustrated in Table 4-3, the carbon concentration in the matrix is about 11.44%, which is much higher than the 4.73wt% carbon concentration measured in the laminate method. The matrix in the composite fabricated by the infiltration method is free from oxygen, while 1.34wt% of oxygen was found in the case of the laminate method. EDX line

mapping is performed to analyse the variation in element content across aluminium matrix, interface and carbon fiber as shown in Figure 4-9.

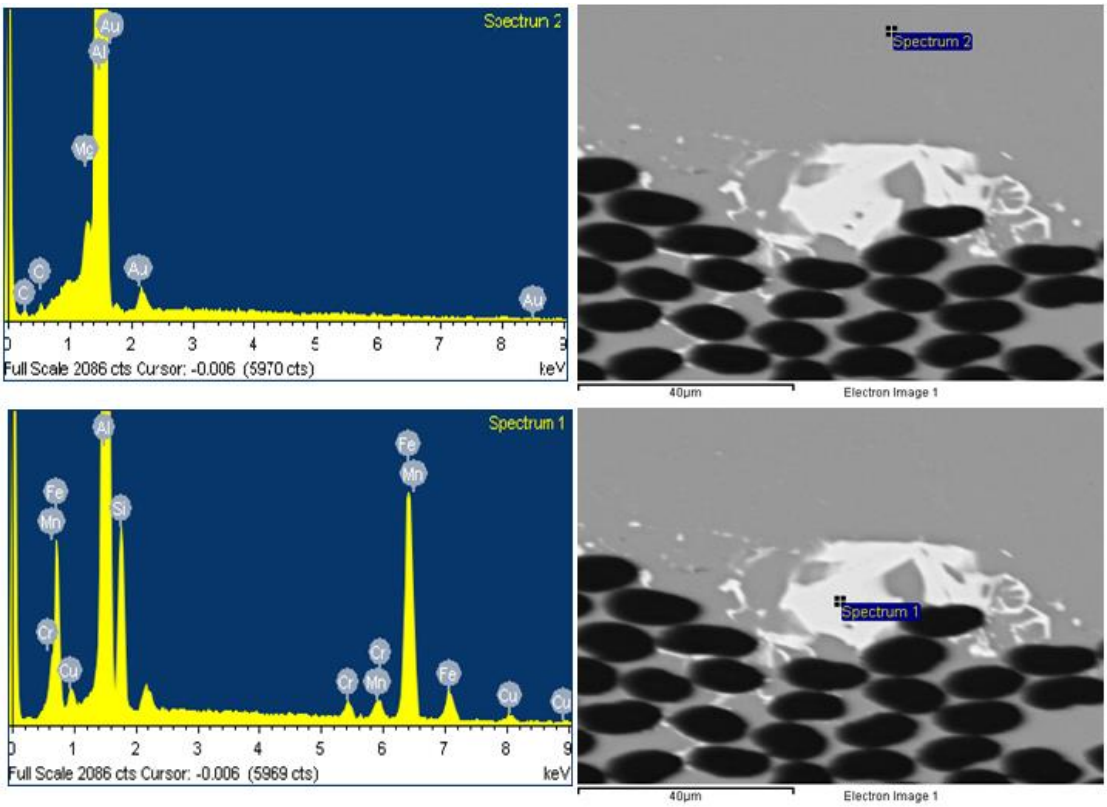

Figure 4-7: EDX analysis at the matrix (top), and at the precipitate (bottom).

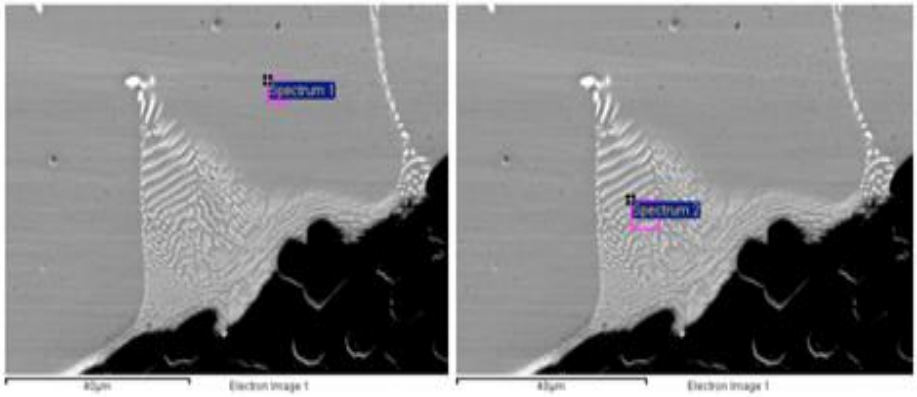

Figure 4-8: EDX analysis at the matrix (left), and at the precipitate (right) (laminate method) [49].

Table 4-3: Element content in the matrix and at precipitates.

Elements	Wt % (Matrix)	Wt % (Precipitate)
C	11.44	5.18
C (Laminate [49]*)*	*4.73*	*3.92*
Al	87.74	65.03
Fe	0	8.32
Fe (Laminate [49]*)*	*0*	*4.31*
Mg	0	0
Mn	0	0.45
Cr	0	0.24
Si	0.81	8.78
Cu	0	1.26
O	0	3.15
O (Laminate [49]*)*	*1.34*	*1.31*
Total	100	100

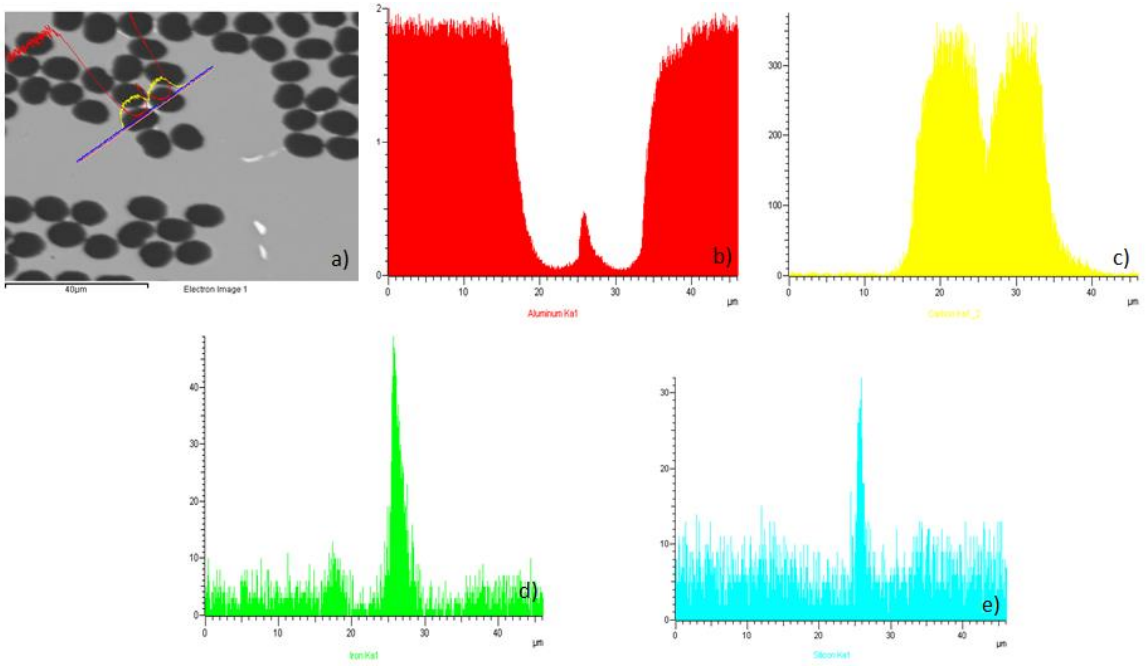

Figure 4-9: EDX along the a) mapped line: element distribution for b) aluminium, c) carbon, d) iron, and e) silicon in sample S_5.

Another type of precipitates is also observed as shown in Figure 4-10. They are relatively darker in appearance than the first type of precipitates. EDX mapping as shown in Figure 4-10 illustrates that this second class of precipitates holds high concentration of oxygen, silicon, and magnesium as tabulated in Table 4-4. In contrast, these second type precipitates are rich in chromium, iron and nickel [49], are needle-like and appeared brighter in the case of the laminate method as illustrated in Figure 4-11 and Table 4-5.

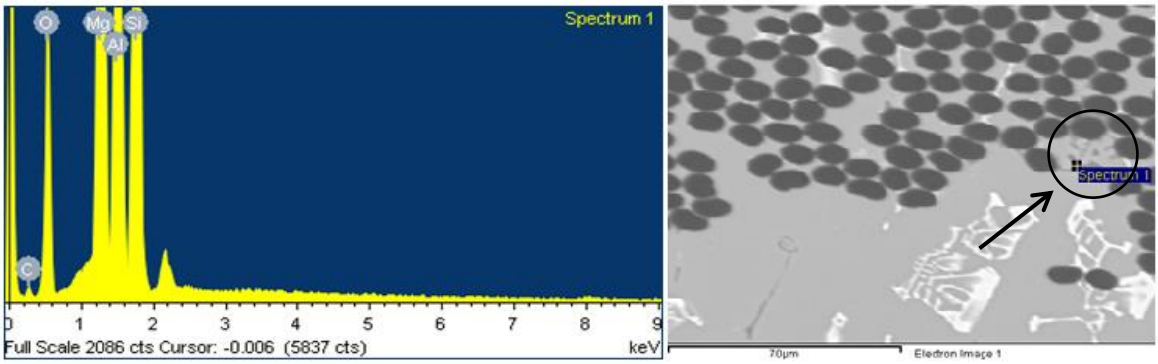

Figure 4-10: EDX mapping of a dark precipitate.

Table 4-4: Chemical composition at secondary (dark) precipitates.

Elements	Wt %
C	7.72
O	33.83
Al	23.42
Mg	16.20
Si	18.84
Total	100

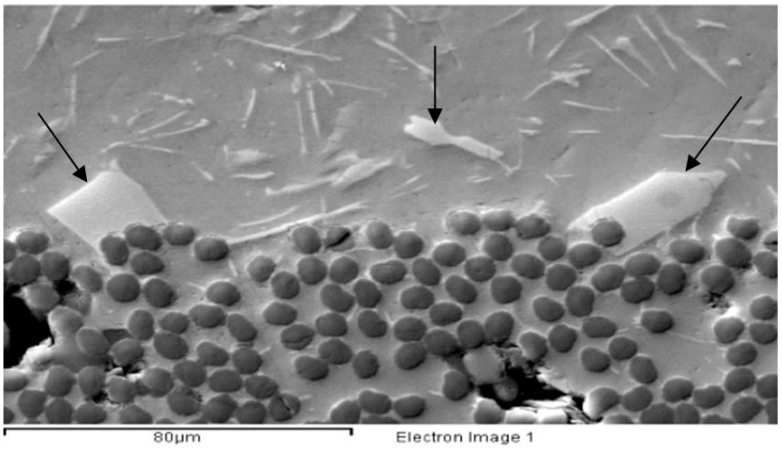

Figure 4-11: Second type precipitates (laminate method) [49].

Table 4-5: Element contents at secondary precipitates (laminate method) [49].

Elements	Wt %
Al	47.09
C	48.70
Fe	1.92
O	1.51
Cr	0.54
Ni	0.24
Total	100

The result of EDX point mapping for 6061 reference aluminium alloy S_A, also fabricated by squeeze casting, is shown in Figure 4-12 and Figure 4-13. As illustrated in Table 4-6, no carbon diffusion from the die material is observed in S_A either in matrix or in precipitates. Also, no other elements are observed except 0.53wt% Mg which is already an inherent element in the base aluminium alloy as shown in Table 3-2. Some precipitates are also observed at grain boundaries in the reference sample. Figure 4-12, Figure 4-13 and Table 4-6 show approximate percentages of the chemical content in these precipitates. Similar to the

composites illustrated in Figure 4-7 and Table 4-3, precipitates with slightly higher contents of silicon, copper, and iron are found in the grain interiors of the base aluminium alloy.

On the other hand, in composites from the laminate method [49], carbon concentrations of 4.87wt% and 4.91wt% were observed in the matrix and at grain boundaries respectively. A considerably higher iron concentration of 18.81wt% was also observed in these precipitates as illustrated in Figure 4-14 and Table 4-7.

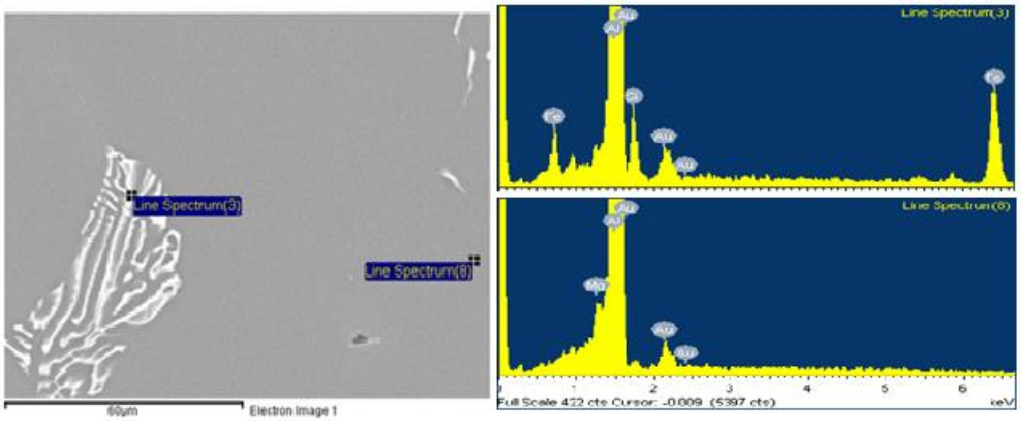

Figure 4-12: Chemical analysis of the base 6061 aluminium alloy S_A.

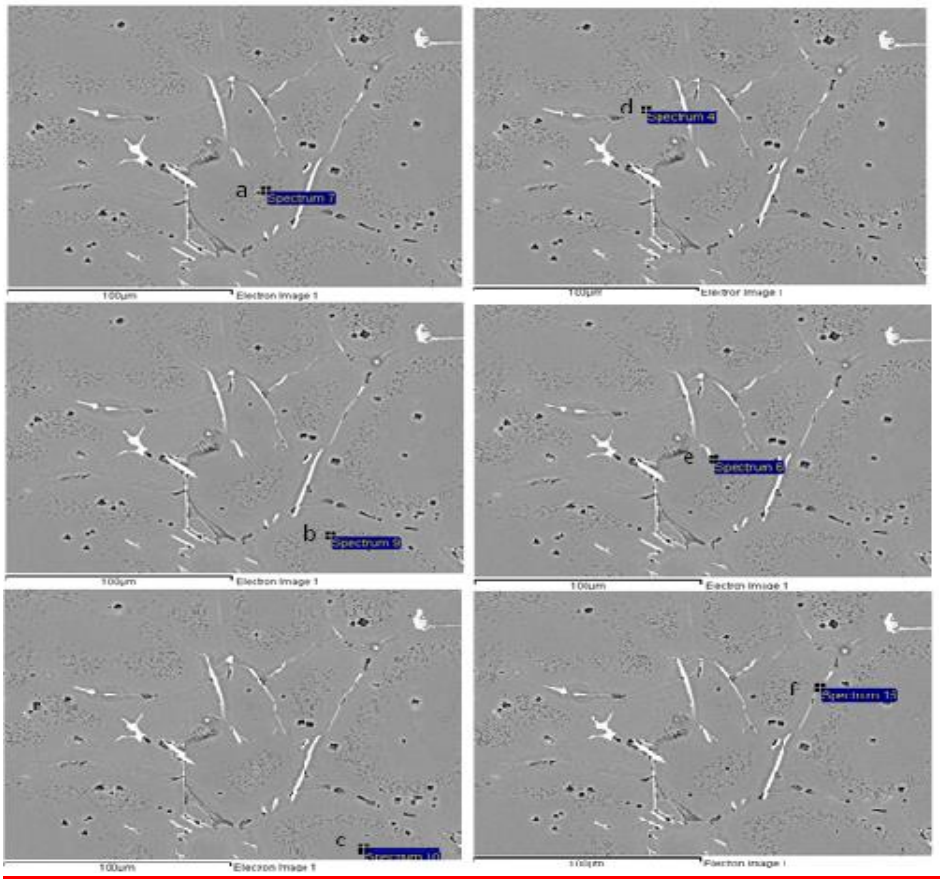

Figure 4-13: Gaunt map analysis in the reference aluminium alloy S_A.

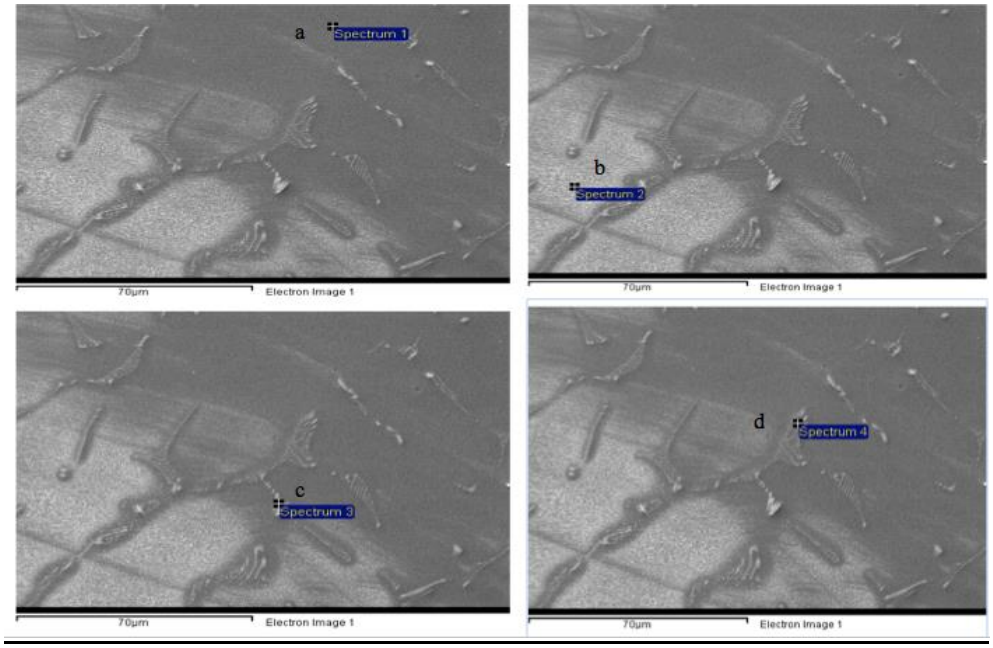

Figure 4-14: Gaunt map analysis in the reference aluminium alloy (laminate method) [49].

Table 4-6: Chemical composition in grain interior and at grain boundary precipitates in the base 6061 aluminium alloy fabricated by the infiltration method.

Elements	Wt % (Matrix)			Wt % (Precipitate)		
	a	b	c	d	e	f
C	0	0	0	0	0	0
Al	99.1	99.5	99.76	97.96	96.13	97.25
Fe	0	0	0	0	0.44	0.43
Mg	0.45	0.5	0.24	0.61	0.38	0.37
Mn	0	0	0	0	0	0
Cr	0	0	0	0	0	0
Si	0.45	0	0	0.79	0.95	0.96
Cu	0	0	0	0.63	0.99	0.99
O	0	0	0	0	1.11	0
Total	100	100	100	100	100	100

Table 4-7: Carbon, iron and oxygen concentrations in grain interior and at grain boundary precipitates in the reference aluminium alloy fabricated by the laminate method [49].

Elements	Wt % (Matrix)	Wt % (Precipitate)
C	4.87	4.91
Fe	--	18.81
O	1.27	--

4.2 Hardness

Vickers hardness measurements at carbon fiber/aluminium matrix interface are summarized in Figure 4-15; both samples S_4 and S_5 show almost identical hardness values which are lower compared to S_1, S_2, and S_3. Figure 4-15 also indicates that the fiber/matrix

interface is harder, when S_5 is compared to the base aluminium matrix alloy and the composites fabricated using the laminate approach.

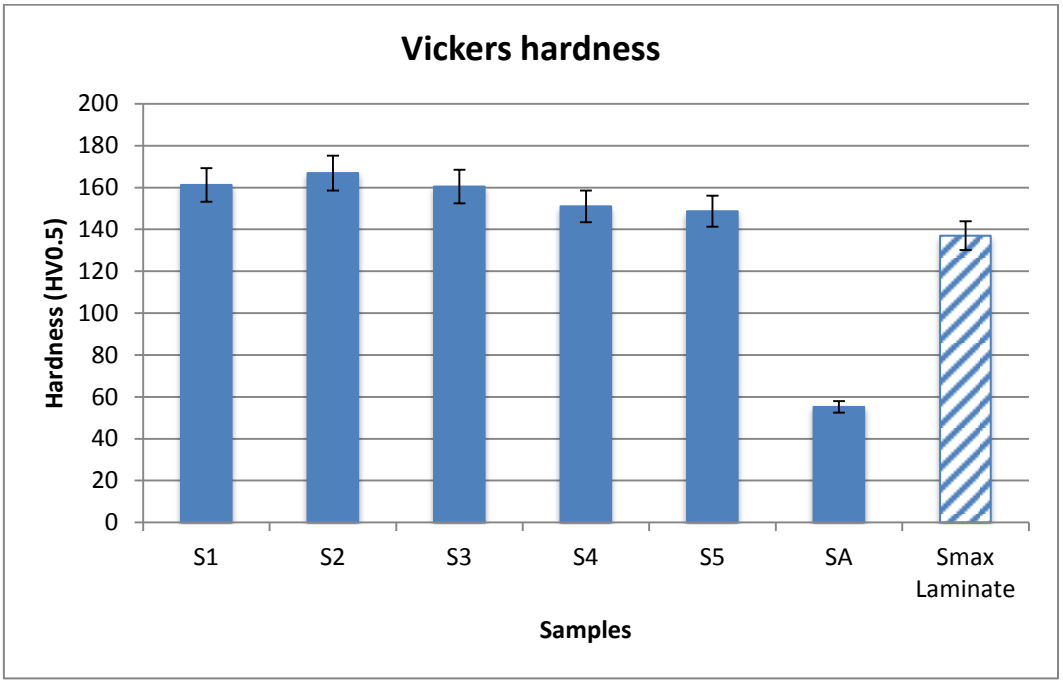

Figure 4-15: Vickers hardness comparison between 6061 aluminium reference and fiber/matrix interfaces of composites fabricated by the infiltration method (S_1, S_2, S_3, S_4 and S_5) and the laminate method.

Rockwell indentation diameters are measured for bulk hardness estimation of the composites. Larger indentations on the samples S_4 and S_5 indicate that they possess low bulk hardness compared to the samples S_1, S_2, and S_3 samples with higher carbon fiber content. Even larger indentation diameters are measured in samples obtained by the laminate method and in the base aluminium alloy which exhibits the lowest bulk hardness. The results are summarized in Figure 4-16.

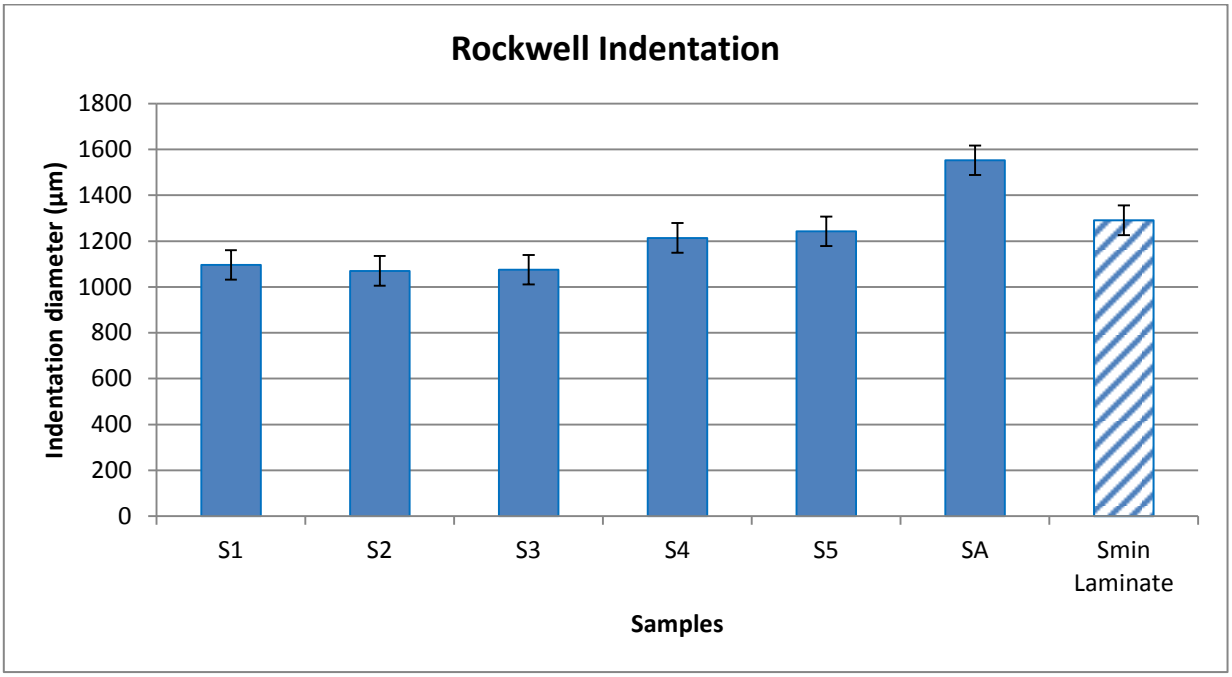

Figure 4-16: Indentation diameter comparison among the fabricated composites, 6061 aluminium reference alloy and laminate composites.

4.3 Bend resistance

Load-deflection curves are shown in Figure 4-17. Samples S_4 and S_5 demonstrate highest bend resistance, while S_1, S_2 and S_3 show low bend resistance when compared to the cast reference aluminium alloy. Initial slops of the elastic region of the curves are calculated in order to evaluate bend moduli as tabulated in Table 4-8. The flexural strength values are also tabulated in Table 4-8. The overall results of the current study show better values in terms of bend strength compared to the best results of the laminate composites.

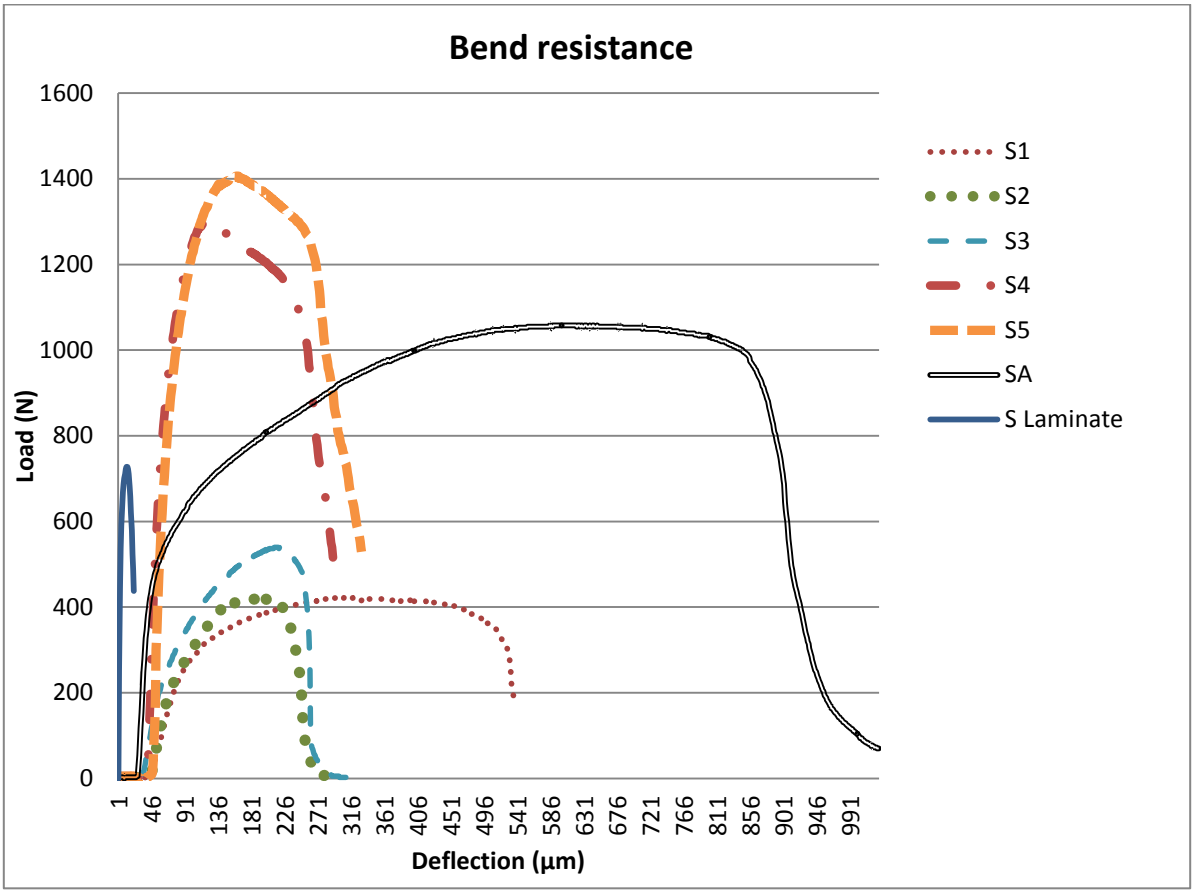

Figure 4-17: Three point bend test curves.

Table 4-8: Sample dimensions and bend moduli for the different composites and the 6061 aluminium reference alloy.

Samples	Thickness 'd' (mm)	Length 'L' (mm)	Width 'b' (mm)	m (P/D)	Flexural modulus 'E' (GP)	Flexural strength (MPa)
S_1	3.64	55	12	480.22	34.51	217.93
S_2	3.64	55	12	583.23	41.91	220.42
S_3	4.11	55	12	723.02	36.10	221.61
S_4	6	55	12	4762.22	76.41	241.58
S_5	6	55	12	4941.20	79.29	267.55
S_A	5.6	55	12	2025.09	39.97	231.80
Laminate method [49]						
Sample	4.33	40	12	4887	80.26	223.16

4.4 Impact toughness

The impact energy absorbed (E_{abs}) during the test and their thickness (t) specific values (E_{abs} / t) are tabulated in Table 4-9 and plotted in Figure 4-18. In general, 6061 aluminium alloy is tougher than all composites and absorbs the largest amount of energy. Overall, samples fabricated by the infiltration method exhibit lower impact toughness compared to the composites fabricated by the laminate approach. Nevertheless, samples S_4 and S_5 exhibit impact toughness values closer to the composites fabricated by the laminate method even though they contain higher carbon fiber volume fractions.

Table 4-9: Impact energy absorbed during Charpy impact test.

Samples	Thickness (t)	Eabs (J)	Eabs/t (J/mm)
S_1	3.64	2.32	0.64
S_2	3.64	4.04	1.11
S_3	4.11	4.89	1.19
S_4	6.00	10.86	1.81
S_5	6.00	11.40	1.90
S_A	5.60	14.33	2.56
Laminate [49]			
Sample	4.33	8.91	2.06

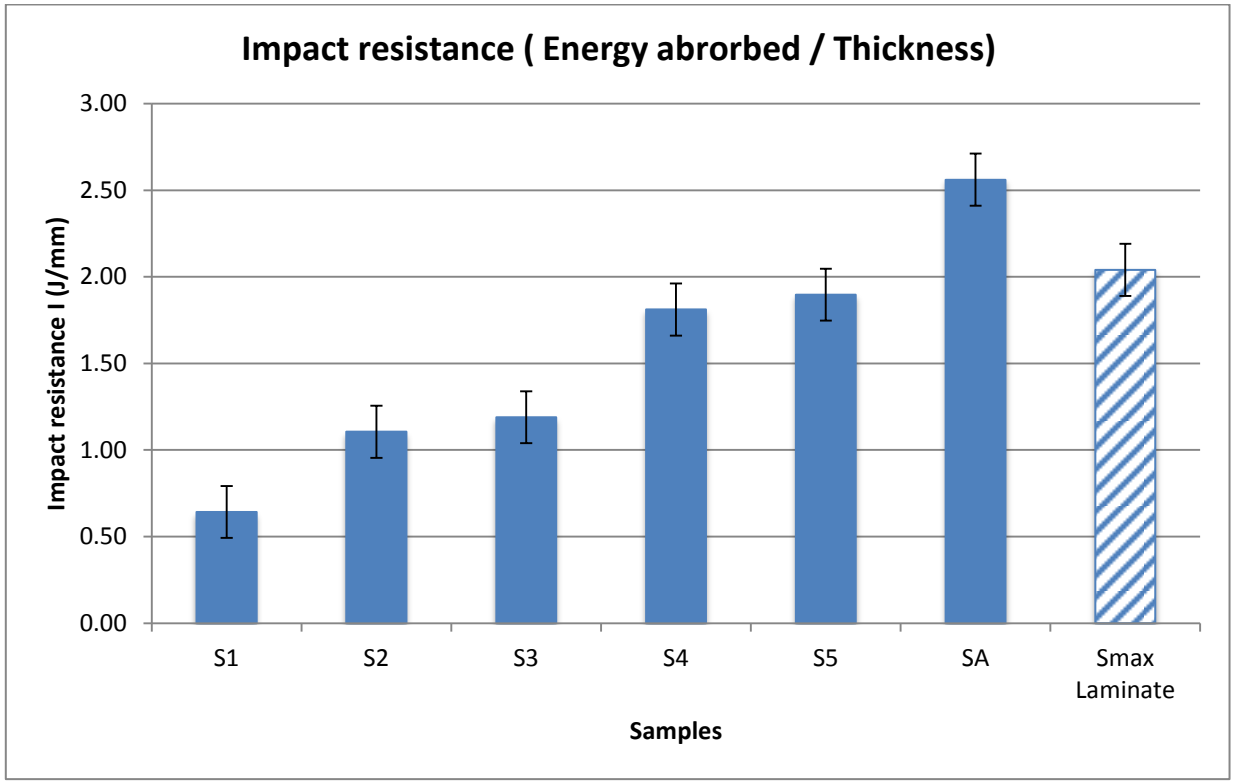

Figure 4-18: Impact fracture energy comparison among the fabricated composites, 6061 aluminium reference alloy and the best sample of the laminate method.

A visual evaluation is performed on fracture surfaces obtained after impact tests. Brittle fracture is characterised by a flat fracture surface through both composite matrix and fibers without any fiber pullout whereas ductile fracture shows relatively rough surface with fiber pullout indicating plastic deformation of the matrix. Based on visual evaluation, it is found that the fracture mode for samples S_1, S_2 and S_3 is 85% brittle and 15% ductile. While the samples S_4 and S_5 are tougher and show fracture surfaces with 75% brittle and 25% ductile fracture proportions as shown in Figure 4-19. Composite materials generally tend to be brittle because of the presence of brittle reinforcement and therefore possess poorer capability to resist impact fracture compared to their ductile matrix. This is primarily due to easy debonding between carbon fiber layers and the aluminium matrix [5] [72].

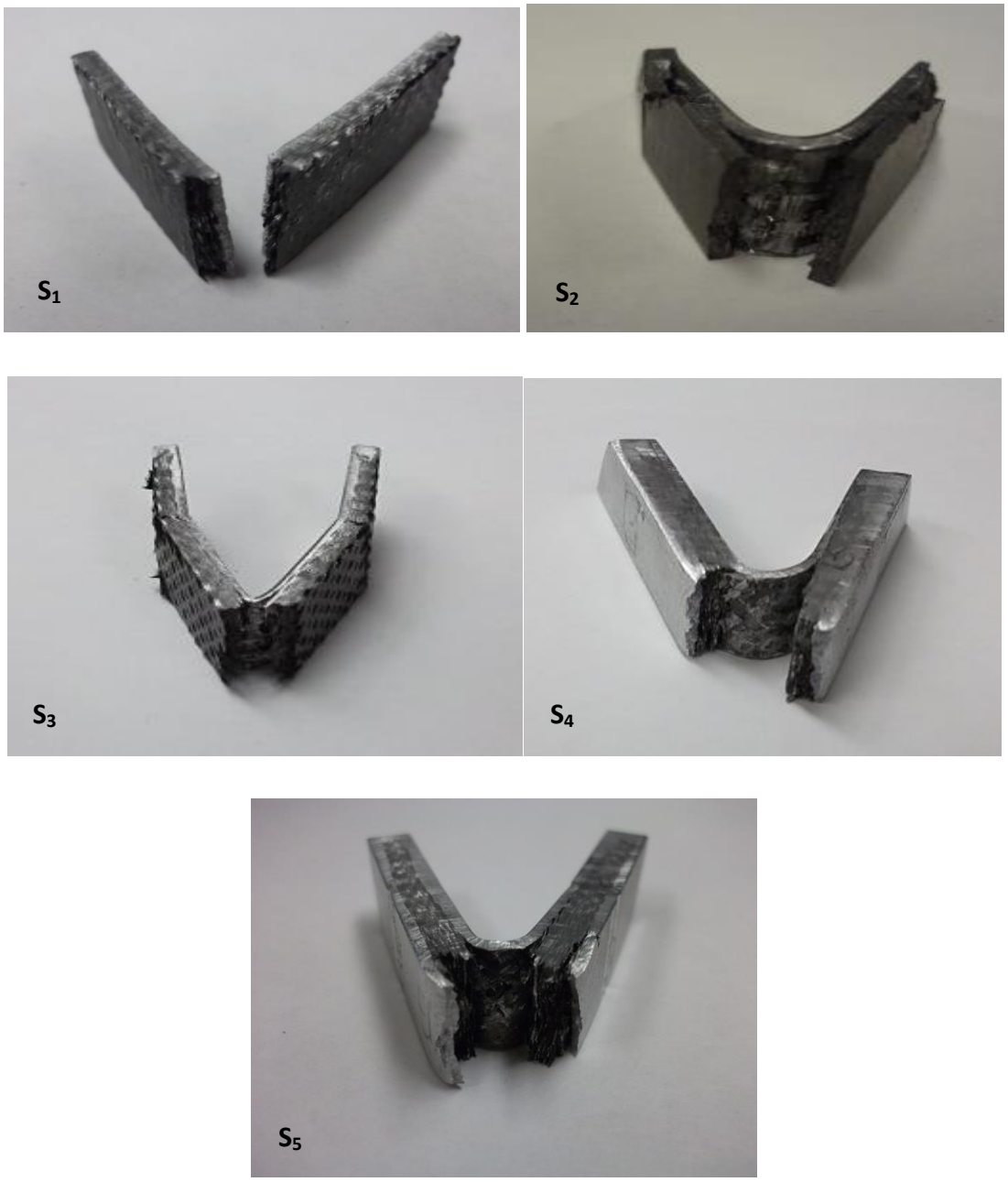

Figure 4-19: Fracture in samples S_1, S_2, and S_3 (85% brittle – 15% ductile); S_4 and S_5 (75% brittle – 25% ductile).

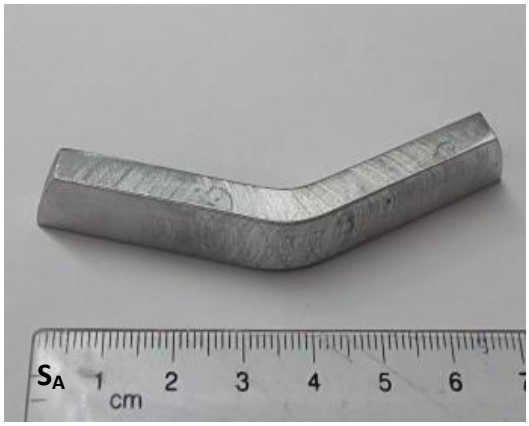

Figure 4-20: Deformation of aluminium 6061 (S_A) upon impact test. No fracture occurs.

5 DISCUSSION

5.1 Interaction between fiber and matrix

The adhesion between the fiber and the matrix is a key factor in the performance of composites. The reaction between the fibers and the liquid metal promotes wetting and strong adhesion. However, it can also produce brittle carbides and reduce the strength of the composites [72]. Therefore, the capacity of the melt to wet the surface of carbon fibers is the key challenge of the fabrication process.

If coating is applied to the fiber in order to increase wettability with the molten aluminium, long liquid/fiber contact time may dissolve the coating material [45]. Therefore, the advantage of the high pressure squeeze casting process is that it reduces contact time through force-infiltration of molten metal into designed preforms leading to rapid solidification. Rapid solidification is achieved by the increase in solidification temperature of the matrix due to high pressure that also increases the rate of heat dissipation through the die. Hence, the squeeze casting technique can significantly reduce fiber/matrix reactions at the interface [45] resulting in increased wettability of aluminium on fiber materials [73]. From the SEM images in the Results section (Figure 4-1 and Figure 4-3), it can be seen that the fiber/matrix boding is primarily of adhesion type and the interface is free from reaction products.

In contrast, because of the long contact time between fiber and aluminium during the heating and cooling cycles in the laminate fabrication process, excessive formation of detrimental Al_4C_3 at the fiber/matrix interface can take place [49] (particularly at 500°C [45]). Also, the presence of an oxide layer over the aluminium foils can provide more oxygen to react

with carbon which can produce carbon monoxide eventually leading to pores at the interface. This reaction is described as:

$$2Al_2O_3 + 9C \rightarrow Al_4C_3 + 6\,CO \quad [49]$$

The presence of oxide may also lead to precipitation of other oxides which is discussed in Section 5.3. The pores at the interface can limit or hinder bonding between fiber and matrix; and thus the strength of the reinforcing fibers cannot be fully utilized in the composites. On the other hand, the oxide layer on aluminium foils seems to also have the advantage of preventing interdiffusion between molten aluminium and carbon fibers. In addition, the formation of Al_4C_3 at the interface seems to consume part of the carbon that diffuses into the molten aluminium. Consequently, lower carbon concentrations are measured in the aluminium matrix in the case of the laminate method. Overall, however, it is established that minimizing the availability of oxygen during fabrication and reducing oxides and carbides at the fiber/matrix interface can substantially improve the quality of the composites.

5.2 Effect of reducing the carbon fiber fabric density

The infiltration of molten aluminium into the carbon fiber fabric can be described by the Darcy's law [3] as:

$$v = -\frac{k}{\mu}.\frac{dP}{dX} \quad [61] \qquad (11)$$

where v is the seepage velocity (m/s); k is the permeability; and μ is the viscosity. The negative sign indicates that the fluid flows from high pressure to low pressure regions. The Darcy's Law implies a uniform (linear) pressure drop along the entire length of the composite as shown in Figure 5-1 [74].

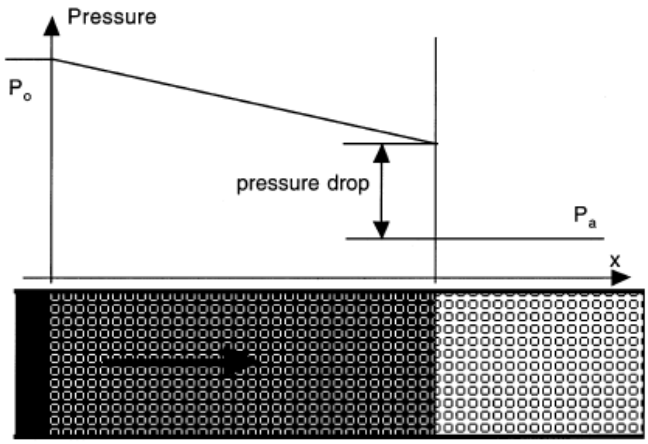

Figure 5-1: Pressure distribution in unidirectional infiltration [75].

Since the viscosity of molten aluminium and the pressure gradient through the fiber fabric are assumed to be constant during infiltration, the Darcy's law can be simplified into a linear proportionality between liquid seepage velocity v and the permeability$k$.

$$v \; \alpha \; k$$

The lower density fabric is approximately two times more permeable than the original fabric as interpreted from Figure 5-2. Therefore, the seepage velocity of the molten aluminium through the reduced fiber fabric can also be expected to be approximately twice that of the original fabric. The carbon fiber content affects the bond strength between the fiber and the matrix by influencing the liquid infusion capability of aluminium into the fiber [74] [76]. In the laminate method, it has been already established that with increasing carbon volume fraction there are more regions that are not properly infused by the matrix resulting in porosity at the interface between the fibers and the aluminium matrix [49]. It has also been demonstrated in the previous study that there is an optimum fiber volume fraction around 45% that provides best mechanical properties. However, this thesis emphasizes that the fabrication process also plays an important role to obtain composites with good fiber/aluminium bonding, minimum defects and porosity; hence, better mechanical properties. This is in agreement with the Darcy's law

that denser carbon fiber fabric leads to more restricted flow of the molten aluminium and to stronger pressure drop during squeeze casting as shown in Figure 5-1. Consequently, it produces weaker fiber/matrix interface and low impact resistance in the final composite. For example, as mentioned in the Results section, samples S_4 and S_5 yield overall improved results including higher modulus of elasticity and impact resistance compared to samples S_1, S_2 and S_3 with higher carbon fiber contents. This is because of the comparatively better matrix infiltration due to much easier flow of the molten matrix into the loose fabric. However, better fluidity of the molten metal and better fiber/matrix adhesion can compensate for higher fiber volume content. Therefore, samples S_4 and S_5 show properties similar to the best samples fabricated by the laminate method (see Table 4-8 for flexural modulus and flexural strength and Figure 4-18 for impact resistance) even though they contain higher carbon volume fractions (see Figure 4-5). An exception is that composites fabricated by the laminate method showed higher modulus of elasticity and impact strength because of their lower fiber volume fraction. Samples S_1, S_2 and S_3 have higher Vickers hardness (see Figure 4-15), smaller Rockwell indentation diameter (see Figure 4-16); but they behave more brittle, absorb only little energy to break (see Figure 4-18) and show low impact strength. This is due to low quality aluminium/fiber interfacial bonding as a result of improper infusion which degrades the load transfer capability of the matrix to the fiber within the composite.

Hardness and toughness are the two main requirements for applications such as armour plates, whereby hardness is the priority for the front impact face and toughness is the priority for the backing face. In this study, the reference aluminium alloy showed higher fracture toughness, but lower hardness and strength. Therefore, the reference aluminium alloy can be considered more appropriate for the backing face, whereas the higher hardness and strength of

composites S_4 and S_5 as demonstrated in Sections 4.2 and 4.3 are an indication that they are more appropriate for the front face of potential gradient composites plates.

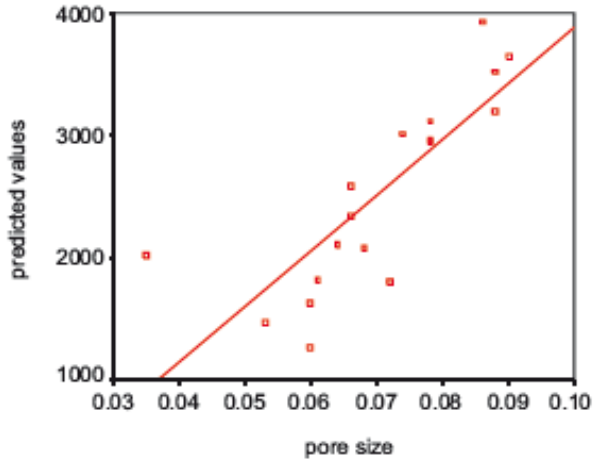

Figure 5-2: Permeability as a function of pore size in woven fabric [77] .

5.3 Formation of precipitates

Precipitates are observed in discrete patches at some locations as bright color interlayers. It has been shown that an increase in carbon concentration in precipitates can be linked to the formation of aluminium carbide crystals as observed using EDX SEM images (Figure 4-6 and Figure 4-7). From the aluminium-carbon phase diagram (Figure 5-3), it is observed that over a wide range of temperature and concentrations, two phases co-exist. One is liquid, that is, aluminium matrix and another is the reaction product, that is, Al_4C_3 which accumulates in the form of precipitates during fabrication [21]. Al_4C_3 is brittle and leads to relatively low impact fracture energy and brittle fracture during Charpy impact tests [21]. It is important to note that the formation of carbides takes place whether air is present or not [72] and the reaction is given as:

$$4\,Al + 3\,C \rightarrow Al_4C_3 \quad [78]$$

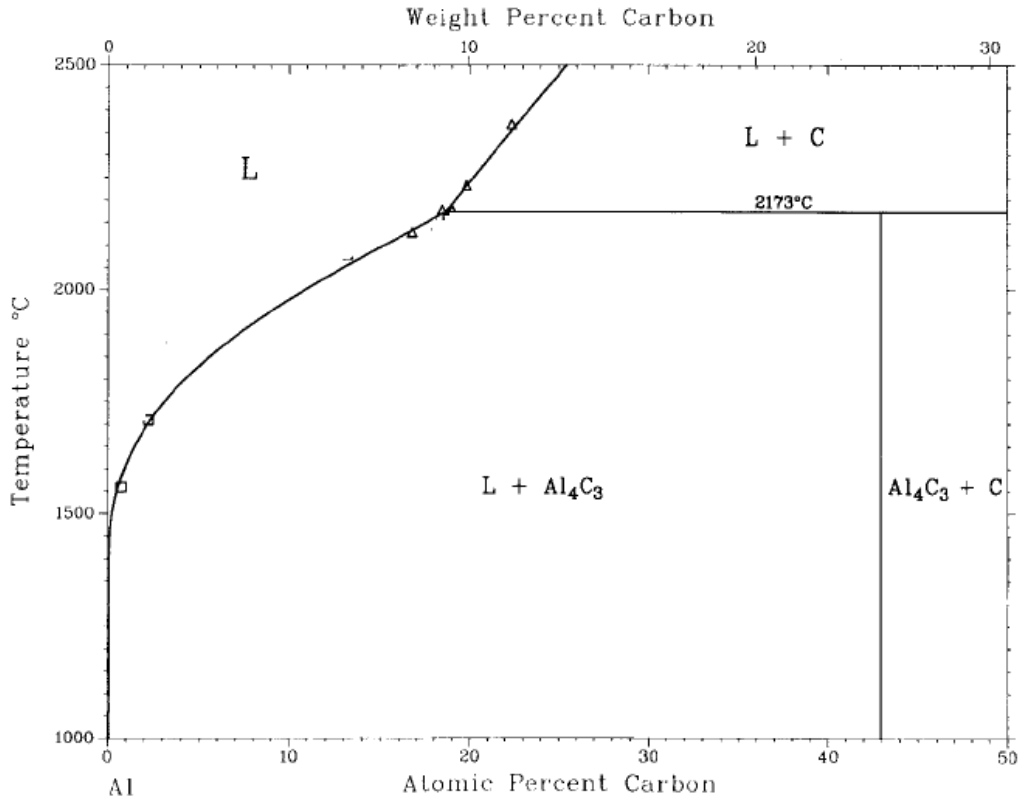

Figure 5-3: Aluminium-carbon phase diagram illustrating the presence of aluminium-carbide in aluminium matrix composites [79].

Beside Al_4C_3, the presence of oxygen in the environment during squeezing leads to oxidation, and hence to the formation of a potential Al_4O_4C phase which can be further detrimental to the composites as demonstrated in the laminate method [49], where Al_4O_4C was reported at the fiber/matrix interface along with Al_4C_3 and CO [49]. The formation of these reaction products is more detrimental at the interface than within the matrix as they cause interfacial debonding and eventually low quality composites. Therefore, it is a great advantage of the liquid infiltration method that such reaction products are substantially reduced. This successfully eliminates excessive oxidation and pores in the casts.

In addition, the presence of Si in aluminium 6061 serves to limit the formation of Al_4C_3. Free Si reacts with C to form SiC and thereby prevents aluminium-carbide formation and

promotes wettability [72]. In contrast, the difference in thermal expansion coefficients between fibers and matrix aluminium causes incoherency or high dislocation density near the fiber/matrix interface. This promotes precipitation reactions as dislocations act as heterogeneous nucleation zones for precipitates [16] [21].

Two other types of precipitates are observed in the composite:

(1) White precipitates that are iron rich and are thought to be iron aluminide (Fe_3Al) (Figure 5-4). They are created by diffusion of iron from the die into the molten aluminium during squeeze casting [49]. These iron aluminide intermetallics form during solidification at temperatures around 550°C to 400°C [80] [81] [82]. They might contain another iron aluminide intermetallic, that is, FeAl supposed to form due to relatively higher iron content over a wide range of temperature as shown in Figure 5-4. Iron-aluminide precipitates were also observed in composites fabricated using the laminate method [49]. However, as observed in Figure 4-8, the precipitates in composites fabricated by the laminate method are lamellar in appearance and are thought to be a eutectic structure composed of Al and $FeAl_3$ layers formed at 660°C and 2wt% Fe (point 'E' in the phase diagram in Figure 5-4).

(2) The dark precipitates shown in Figure 4-10 are rich in oxygen, silicon, magnesium, and carbon. Their element concentrations are tabulated in Table 4-4.

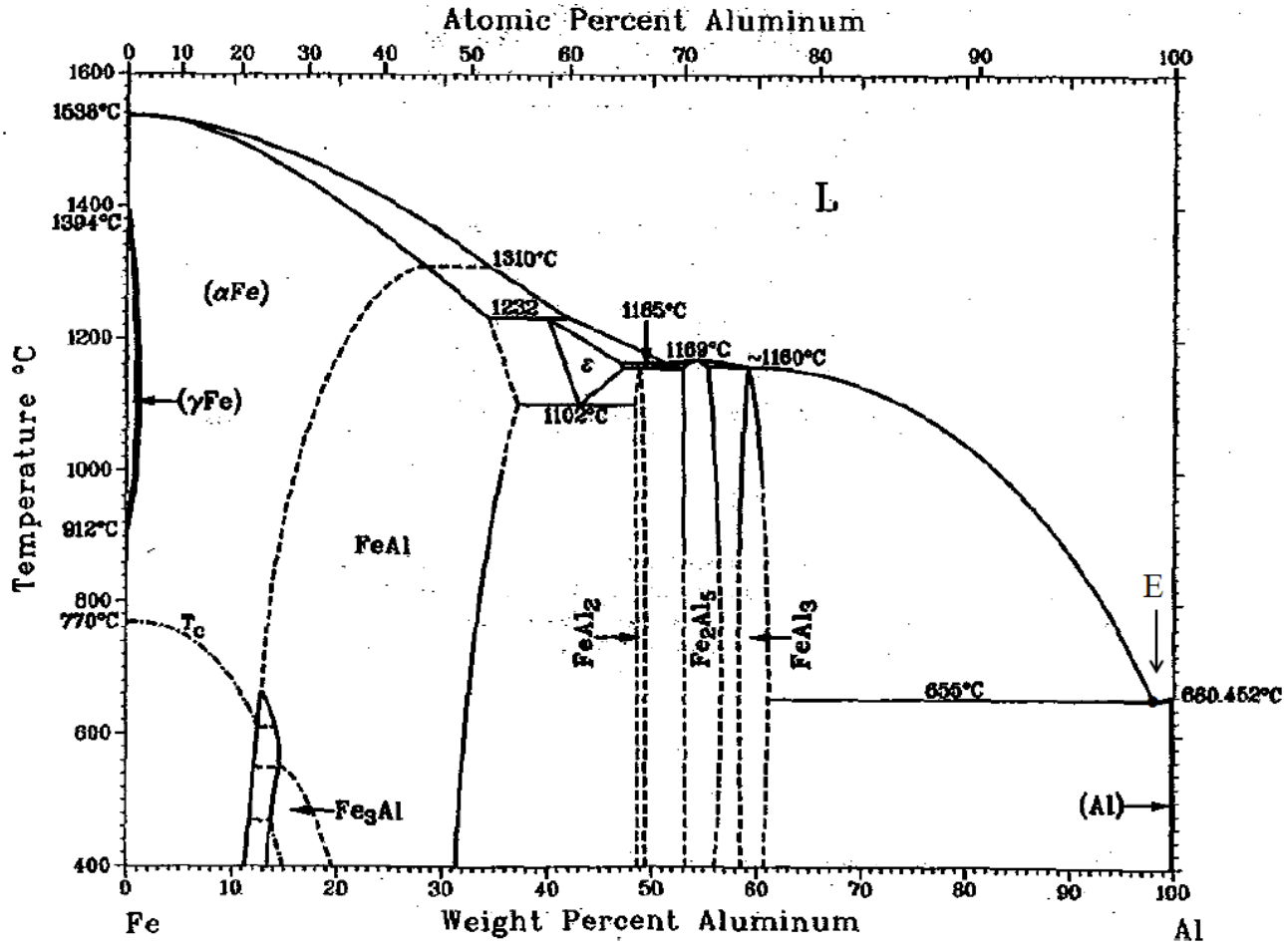

Figure 5-4: Iron-aluminium binary phase diagram [80].

Again, carbon obviously originates from the fibers and/or the crucible during casting. Silicon and magnesium can be linked to their respective oxides. Silicon possesses strong affinity with oxygen which produces SiO_2 [83]. In this thermal oxidation process, silicon reacts with either oxygen or water vapour present in the furnace, and also during squeezing when the temperature is above 600°C, to form silicon dioxide. The reaction can be described as [84]:

$$Si + O_2 \rightarrow SiO_2$$

$$Si + 2H_2O \rightarrow SiO_2 + 2H_2$$

The products of the reactions between SiO_2 and molten aluminium containing Mg may be Al_2O_3, MgO, $MgAl_2O_4$. For high Mg concentrations, MgO can be expected, whereas for low

concentrations of Mg, $MgAl_2O_4$ can be expected [85]. Precipitates may also contain reaction products such as Mg_2Si [85]. Al_2O_3 may also be present as a metallurgical inclusion due to contact of molten aluminium with ambient air. Alumina (Al_2O_3) may undergo reduction reaction with carbon to produce Al_4C_3, therefore may be considered as secondary source of Al_4C_3. The reaction can be described as:

$$2\ Al_2O_3 + 9\ C \rightarrow Al_4C_3 + 6\ CO \quad [86]$$

The reference aluminium casting also contains some precipitates; their composition is listed in Table 4-6. These precipitates are rich in magnesium, silicon and copper. They may also be oxides of magnesium and silicon similar to those in composites. The presence of copper can be linked to stable intermetallics such as Al_2Cu [87]. Similarly, some oxides were noticed in composites fabricated by the laminate method [49].

5.4 Physics based calculation of composite properties

Simple but important physical properties such as elastic modulus, flexural strength and density are calculated and compared with experimental values. The modulus of elasticity of composites (E_c) can be estimated by using the rule of mixture for carbon fibers (*f*) and aluminium matrix (*m*) as:

$$E_c = E_f V_f + E_m V_m$$

where E_f = 231 GPa and E_m = 69 GPa (Table 3-1); V_f = 0.647 for S_5 (Figure 4-5), and $V_m = 1 - V_f$ = 0.353

yielding:

$$E_c = (231)(0.647) + (69)(0.353)$$

$$E_c = 174.3 \text{ GPa}$$

The experimental value of the modulus of elasticity is computed to be 79.29 GPa for S_5 (Table 4-8) which is 2.19 times lower than the theoretical composite value and only slightly higher than the aluminium matrix elastic modulus.

Similarly, the rule of mixture can be applied to the flexural strength of the composites as:

$$\sigma_c = \sigma_f V_f + \sigma_m V_m$$

where $\sigma_f = 1810$ MPa [88], and $\sigma_m = 231.80$MPa (Section 4.3)

yielding for S_5:

$$\sigma_c = (1810)(0.647) + (231.80)(0.353)$$

$$\sigma_c = 1252.8 \text{ MPa}$$

The experimental value of the flexural strength of the composite is computed to be 267.55 MPa for S_5 (Section 4.3). This value is 4.7 times lower than the theoretical composite value and slightly higher than the aluminium matrix strength.

These discrepancies between theoretical and experimental values can be linked to fiber pullout from the matrix during loading because of precipitates that weaken the fiber/matrix bond and cause crack initiation and propagation [89]. Also, the elastic modulus is known to be very sensitive to pre-existing cracks developed during fabrication and the increase in crack density during nucleation and coalescence [90].

Similarly, the density of the composites can be estimated as:

$$\rho_c = \rho_f V_f + \rho_m V_m$$

where ρ_f = 1.79 g/cm^3 (Table 3-3), and ρ_m = 2.7 g/cm^3(Table 3-1)

yielding for S_5:

$$\rho_c = (1.79)(0.647) + (2.7)(0.353)$$

$$\rho_c = 2.14 \text{ g/cm}^3$$

The actual density of the fabricated composite is measured by dividing the weight of the composite by its volume to be 2.21 g/cm^3 for S_5 which is slightly higher than the calculated theoretical value from the rule of mixture. This difference in density may be due to the diffusion of iron with higher density from the die, which is in agreement with the observed precipitation of iron aluminide intermetallics as already discussed in Section 5.3. The atomic weights of iron, aluminium and carbon are 55.845, 26.9815 and 12.0107 respectively [91]. So, iron is 2.06 and 4.65 times heavier than aluminium and carbon respectively. Therefore, its addition into the composite can well be expected to increase the composite density.

5.5 Manufacturing defects

Changes were made with respect to the previous work [49] in order to reduce manufacturing defects. First, graphite used as lubricant in the laminate method was shown to be an additional source of carbon diffusion into the composite [49]. Therefore, Boron Nitride (white graphite) supplied by Slide, USA, is used in this study.

The physical properties of aluminium matrix composites are tailored by appropriate types, content and configuration of fiber as well as by the method of fabrication. The method of fabrication dictates several aspects such as formation of precipitates, phase changes, and chemical reactions which govern the quality of the composite. The manufacturing method and phase transformations upon cooling can produce considerable residual stresses in composites. In this study, the composites are subjected to the fabrication temperature of 850°C. Therefore, large thermal stresses are developed as a result of excessive shrinkage during cooling and solidification of the aluminium matrix. These stresses cause substantial plastic deformation of the matrix and/or relative sliding between fiber and matrix at the fiber/matrix interface. This relative sliding can cause interfacial debonding of the fibers from aluminium leading to a reduction in elastic modulus and premature fracture of the composites [1]. The thermal stresses

generate during cooling either from temperature gradients within the composite and/or from a mismatch of coefficients of thermal expansion (CTE) between the matrix and the reinforcement. The effect of temperature gradient can be minimized by slow and steady cooling of the material. But the mismatch of CTE is inherent to composites as multiphase materials; therefore, it cannot be addressed through modifications of the manufacturing method but rather by appropriate selection of matrix and fiber compositions. The difference in CTEs in metal matrix composites is generally large. For example, in aluminium matrix composites the CTE of Al is $25x10^{-6}$/K [1] and the CTE of PAN-based carbon fibers is only $15x10^{-6}$/K [92]. Hence, upon cooling, aluminium undergoes larger contraction compared to the fibers leading to tensile residual stresses in aluminium because of higher coefficient of thermal expansion and compressive residual stresses in the fiber because of lower coefficient.

Inclusions and precipitates are locations of stress and deformation concentration and therefore promote crack nucleation and propagation.

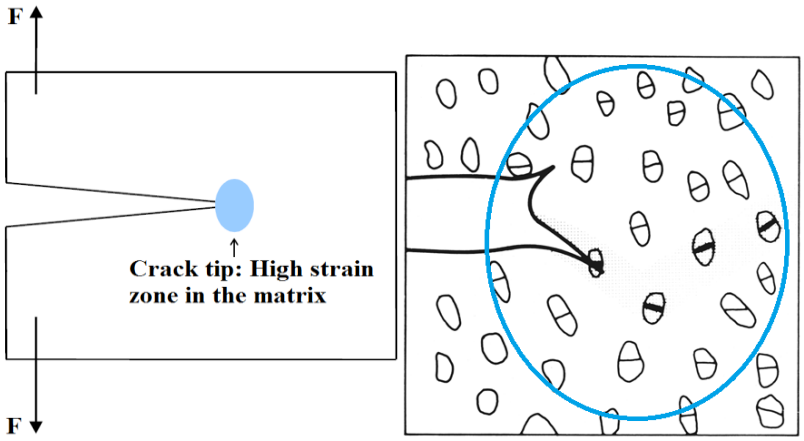

Figure 5-5: Schematic representation of a crack tip high strain zone and cracks in precipitates/inclusions in the highly deformed region [93] [94].

In fact, precipitates in the vicinity of the plastic deformation zone undergo interface decohesion with the matrix. Therefore, these inclusions provide the primary nucleation sites for the

formation and growth of cavities by coalescence. This degrades the toughness of composites as compared to its matrix alloy fabricated under identical conditions as demonstrated in Figure 4-15. Overall, the distribution and amount of heterogeneous phases affect the toughness of the composites [93].

6 CONCLUSIONS

Carbon fiber reinforced aluminium matrix composites are successfully manufactured by the squeeze casting infiltration process. The resulted composites show improved properties as follows:

1) The fiber/matrix bond is primarily of adhesion type and the interface is free from reaction products. In this process, liquid pressure during cooling and low liquid viscosity promote strong fiber/matrix bonding.
2) The lack of spacers between the fiber fabric layers produces aluminium matrix composites with overall higher fiber volume fraction compared to the laminate method**.**
3) Liquid infiltration produces overall higher hardness at fiber/matrix interfaces. Properly infiltrated sample (S_5) shows 8.52% higher hardness than the composite fabricated by the laminate method. Similarly, the composites fabricated by liquid infiltration experience 3.71% lower indentation diameter (bulk hardness) than the composite fabricated by the laminate method. Both methods produce higher hardness compared to the reference 6061 aluminium alloy casted under identical conditions.
4) The flexural strength of the composites is increased by 19.9% compared to the laminate approach probably due to higher fiber contents. The flexural strength of the composites is also increased by about 15.4% compared to that of the reference 6061 aluminium alloy squeeze casted under identical conditions.
5) Composites by liquid infiltration possess overall lower modulus of elasticity, indicating that they are less stiff compared to composites fabricated by the laminate method.

6) A reduction in impact strength of 7.76% is observed compared to the composites fabricated by the laminate method. The impact strength is reduced by 25.78% when compared with the reference aluminium alloy.
7) Increase in stiffness and in impact strength is achieved with reduced fiber fabric (reducing fiber volume fraction by 3.7%, compared with composites having original fiber) which demostrates that further reducing the fiber volume fraction to the optimum value [36] [45] of about 45% [49] may further:
    a. improve wettability
    b. provide thorough infiltration
    c. give better fiber/matrix interface
    d. produce better composites in terms of toughness due to thorough impregnation of fibers by molten aluminium

Overall, the liquid impregnation method prevents excessive oxidation and miniminzes brittle phase formation due to shorter fiber/molten aluminium contact time which are major advantages compared to the laminate method. However the fiber volume fractions are too high and need to be further reduced.

7 FUTURE WORK

The current work completes a comparative investigation of two fabrication methods for carbon fiber reinforced aluminium matrix composites: (1) the liquid infiltration and (2) the laminate squeeze casting methods. Future work will focus on gradient composite materials manufacture and characterization.

In gradient composite materials, fiber concentration, microstructure and properties will be varied across the thickness from one face to the other. The comparative investigation showed that while forced liquid infiltration provides better impregnation of the carbon fibers by liquid aluminium resulting in composites with far less porosity, the laminate method allows greater flexibility and control over the microstructure across the composite thickness.

On one hand, reactions and oxidation shall be further limited for the laminate method for instance by melting in a vacuum furnace in order to improve resulting composite properties. On the other hand, means of appropriately spacing the single fiber fabric layers shall be found for the liquid infiltration method in order to further reduce the fiber volume concentration in the composites.

Inter-diffusion of carbon from crucible to the matrix of composites can be minimized by using crucible of different material or by using ceramic lined crucible.

Overall, combining the advantages of both techniques can contribute to improved properties as well as increased control over properties across the thickness for advanced gradient composites for armour applications.

8 REFERENCES

[1] S. Suresh, A. Mortensen and A. Needleman, Fundamentals of Metal Matrix Composites, Butterworth-Heinmann, 1993.

[2] F. C. Campbell, "Introduction to Composite Materials," in *Structural Composite Materials*, ASM International, 2010, pp. 1-30.

[3] A. George, *Thesis: Optimization of Resin Infusion Processing for Composite Materials: Simulation and Characterization Strategies,* Institute of Aircraft Design, University of Stuttgart, 2011.

[4] B. Harris, Engineering Composite Materials, London: The Institute of Materials, London, 1999.

[5] T. Shalu, E. Abhilash and M. Joseph, "Development and Characterization of Liquid Carbon Fiber Reinforced Aluminium Matrix Composites," *Journal of Materials Processing Technology,* vol. 209, pp. 4809-4813, 2009.

[6] A. N. Palazotto, R. Run and G. Watt, "Introduction to Metal Matrix Composites in Aerospace Applications," *Journal of Aerospace Engineering,* vol. 1, no. 1, pp. 3-17, 1988.

[7] ATSB, "Fiber Composite Aircraft - Capability and Safety," Australian Transport Safety Bureau, 2007.

[8] R. Montanari, Advances in Metal Matrix Composites, Switzerland, 2011.

[9] A. Kelly, Concise Encyclopedia of Composite Materials, Revised ed., Pergamon, 1994.

[10] D. Lloyd., "Particle Reinforced Aluminium and Magnesium Metal Matrix Composite Material," *International Materials Reviews,* vol. 39, no. 1, pp. 1-23, 1994.

[11] W. Fei, H. Yue and L. Wang, "Equicohesive Temperature of the Interface and Matrix and its Effect on the Tensile Plasticity of Al18B4O33 Whiskers Reinforced Aluminium Composite at Elevated Temperatures," *Materials Chemistry and Physics*, vol. 119, no. 3, pp. 515-518, 2010.

[12] J. H. Jang and K. S. Han, "Fabrication of Graphite Nanofibers Reinforced Metal Matrix Composites by Powder Metallurgy and Their Mechanical and Physical Characteristics," *Journal of Composite Materials*, vol. 41, no. 12, pp. 1431-1443, 2007.

[13] S. Tjong, "Recent Advances in Discontinuously Reinforced Aluminium Based Metal Matrix Nanocomposites," in *Composite Materials Research Progress*, New York, Nova Science Publishers, Inc., 2008, pp. 275-296.

[14] L. H. Peebles, Carbon Fibers: Formation, Structure, and Properties, Florida: CRC Press, Inc., 1995.

[15] H. Chen and A. Alpas, "Wear of Aluminium Matrix Composites Reinforced with Nickel-Coated Carbon Fibers," *Wear*, vol. 192, no. 1-2, pp. 186-198, 1996.

[16] T. Lim, Y. Kim, C. Lee and K. Han, "Fabrication and Mechanial Properties of Aluminum Matrix Composites," *Journal of Composite Materials*, vol. 26, no. 7, pp. 1062-1086, 1992.

[17] W. D. J. Callister, Materials Science and Engineering: An Introduction, 6th ed., USA: John Wiley & Sons, Inc., 2003.

[18] L. Froyen and B. Verlinder, "Aluminium Matrix Composite Materials, Talat Lecture 1402," EAA - European Aluminium Association, 1994.

[19] J. Kaczmar, "The Production and Application of Metal Matrix Composite Materials,"

Journal of Materials Processing Technology, vol. 106, no. 1-3, pp. 58-67, 2000.

[20] S. Prabu, "Influence of Stirring Speed and Stirring Time on Distribution of Particles in Cast Metal Matrix Composites," *Journal of Materials Processing Technology,* vol. 171, no. 2, pp. 268-273, 2006.

[21] J. I. Song and K. Han, "Mechanical Properties and Solid Lubricant Wear Behavior of Al/Al2O3/C Hybrid Metal Matrix Composites Fabricated by Squeeze Casting Method," *Journal of Composite Materials,* vol. 31, no. 4, pp. 316-344, 1997.

[22] K. V. Mahendra and K. Radhakrishna, "Characterization of Stir Cast Al-Cu-(fly ash + SiC) Hybrid Metal Matrix Composites," *Journal of Composite Materials,* vol. 44, no. 8, pp. 989-1005, 2009.

[23] S. Chand, "Carbon Fibers for Composites," *Journal of Materials Science,* vol. 35, pp. 1303-1313, 2000.

[24] C. H. J. William, "Commercial processing of metal matrix composites," *Materials Science and Engineering,* pp. 75-79, 1998.

[25] L. Gomez, "Analysis of Boron Carbide Aluminum Matrix Composites," *Journal of Composite Materials,* vol. 43, no. 9, pp. 987-995, 2009.

[26] K. U. Kainer, Metal Matrix Composites: Custom-Made Materials for Automotive and Aerospace Engineering, illustrated ed., K. U. Kainer, Ed., Wiley-VCH, 2006.

[27] A. Manna, H. S. Bains and P. B. Mahapatra, "Experimental Study on Fabrication of Al-Al2O3/Grp Metal Matrix Composites," *Journal of Composite Materials,* vol. 45, no. 19, pp. 2003-2010, 2011.

[28] M. W. Barsoum, Fundamentals of Ceramics, IoP, 2003.

[29] S. K. Mital, P. L. N. Murthy and C. C. Chamis, "Micromechanics for Ceramic Matrix Composites via Fiber Substructuring," *Journal of Composite Materials,* vol. 29, no. 614, p. 22, May 1995.

[30] C. H. Andersson, "Flexible Composites, Strength, Deformation, and Fracture Processes. Reinforcement Structures and Tensile Strength," *Mechanics of Composite Materials,* vol. 34, no. 6, pp. 525-536, 1998.

[31] M. Taya, "Strengthening Mechanisms of Metal Matrix Composites," *Materials Transactions, JIM,* vol. 32, no. 1, pp. 1-19, 1991.

[32] D. W. Bennett, *Thesis: Multi-Scale Indentation Hardness Testing; A Correlation and Model,* Texas: A&M University, 2008.

[33] Y. Shen and N. Chawla, "On the Correlation Between Hardness and Tensile Strength in Particle Reinforced Metal Matrix Composites," *Material Science and Engineering,* vol. 297, no. 1, pp. 44-47, 2001.

[34] P. Zhang, S. Li and Z. Zhang, "General Relationship Between Strength and Hardness," *Materials Science and Engineering A,* vol. 529, pp. 62-73, 2011.

[35] K. H. W. Seah, S. Sharma and M. Krishna, "Mechanical Properties and Fracture Mechanism of ZA-27/TiO2 Particulate Metal Matrix Composites," *Journal of Materials Design and Applications,* vol. 217, no. 201, pp. 89-96, 2003.

[36] R. Pereyra and Y. L. Shen, "Characterization of Indentation-Induced 'Particle Crowding' in Metal Matrix Composites,," *International Journal of Damage Mechanic,* vol. 14, no. 197, pp. 40-48, 2005.

[37] M. M. Yovanovich, "Micro and Macro Hardness Measurements , Correlations , and

Contact Models," *44th AIAA Aerospace Sciences Meeting and Exhibit,* no. January, pp. 1-28, 2006.

[38] Wilson Inc., A Division of Illinois Tool Works. *Tukon1102/1202,* MA, 2012.

[39] B. L. Froyen, "Aluminium Matrix Composite Materials, Talat Lecture 1402," EAA - European Aluminium Association, 1994.

[40] www.me.mtu.edu. [Online]. Available: http://www.me.mtu.edu/~mavable/Book/Chap3.pdf. [Accessed 10 November 2011].

[41] H. C. Tsai, A. M. Arocho and L. W. Gause, "Prediction of Fiber/Matrix Interphase Properties and their Influence on Interface Stress, Displacement and Fracture Toughness of Composite," Naval Air Development Centre, Warminster, 1990.

[42] V. Okhuysen, "A Practical Assesment of Fiber Reinforced Aluminium Matrix Composites," *Materials Processing Technology,* vol. 3, pp. 235-265, 2004.

[43] V. Scott, "Interface Microstructures in Fiber-Reinforced Aluminium Alloys," *Composites Science and Technology,* vol. 42, no. 1-3, pp. 251-273, 1991.

[44] J. Hashim, L. Looney and M. Hashmi, "Metal Matrix Composites: Production by the Stir Casting Method," *Journal of Materials Processing Technology,* vol. 92-93, pp. 1-7, 1999.

[45] R. Bhagat, M. Amateau and J. Conway *et al.*, "Squeeze Cast Metal Matrix Composites: Evaluation of Their Strength, Damping Capacity and Corrosion Resistance," *Journal of Composite Materials*, vol. 23, no. 9, pp. 961-975, 1989.

[46] X. L. Roy, B. Vikram and Z. Wei-Hong *et al.*, "Mechanical Property Characterization of a Polymeric Nanocomposite Reinforced by Graphitic Nanofibers with Reactive Linkers,"

*Journal of Composite Materials,*vol. 38, no. 18, pp. 1563-1582, 2004.

[47] S. Kalpakjian and S. R. Schmid, "Manufacturing Engineering and Technology," 5th ed., Pearson Prentice Hall, 2006.

[48] L. Dobrzanski, M. Kremzer and A. Nagel, "Application of Pressure Infiltration to the Manufacturing of Aluminium Matrix Composite Materials with Different Reinforcement Shape," *Journal of Achievements in Materials and Manufacturing Engineering,* vol. 24, no. 2, pp. 183-186, 2007.

[49] H. A. Alhashmy, *Thesis: Fabrication of Aluminium Matrix Composites by Squeeze Casting Technique Using Carbon Fiber as Reinforcement,* Ottawa: University of Ottawa, 2012.

[50] M. B. Karamis, "An Evaluation of the Macro Damage on Metal Matrix Composites after High Velocity Impact," *Journal of Compostie Materials*, vol. 41, no. 3, pp. 1-10, 2007.

[51] J. I. Song and K. S. Han, "Mechanical Properties and Solid Lubricant Wear Behavior of $Al/Al_2O_3/C$ Hybrid Metal Matrix Composites Fabricated by Squeeze Casting Method," *Journal of Composite Materials*, vol. 31, no. 4, pp. 316-344, 1997.

[52] S. N. Ahmad, J. J.Hashim and M. I. Ghazali, "The Effects of Porosity on Mechanical Properties of Cast Discontinuous Reinforced Metal Matrix Composites," *Journal of Composite Materials*, vol. 39, no. 5, pp. 451-466, 2005.

[53] ASM, ASM Handbook: Powder Metal Technnologies and Applications, vol. 7, ASM International, 1998.

[54] V. M. Dekov, V. Arnaudov and F. Munnik *et al.*, "Native Aluminium: Does it Exist?," *American Mineralogist,* vol. 94, pp. 1283-1286, 2009.

[55] EAA, "European Aluminium Association," [Online]. Available: http://www.alueurope.eu/about-aluminium/properties/. [Accessed 26 June 2012].

[56] ASM, "ASM Aerospace Specification Metal Inc.," [Online]. Available: http://asm.matweb.com/search/SpecificMaterial.asp?bassnum=MA6061t6. [Accessed 24 Jan 2013].

[57] Zoltek, "How Is It Made? | Zoltek," [Online]. Available: http://www.zoltek.com/carbonfiber/how-is-it-made/. [Accessed 13 June 2012].

[58] Hexcel, "Carbon Fiber Reinforcements," 13 June 2012. [Online]. Available: http://www.hexcel.com/products/industries/icarbon-fiber. [Accessed 13 June 2012].

[59] S. V. Hoa, Principles of the Manufacturing of Composite Materials, DEStech Publications, 2009.

[60] Elite, "Carbon Fiber Fabric," [Online]. Available: http://www.elitecarbonfabrics.com/carbon-fiber-fabric-products.html. [Accessed 16 June 2012].

[61] F. Robitaille, "Lecture Notes," *Introduction to Composite Materials*, 2012.

[62] Hexcel, "HexTow AS4 Carbon Fiber: Product Data," Hexcel Corporation, Connecticut, 2012.

[63] M. F. McGuire, Stainless Steels for Design Engineers, ASM International, 2008.

[64] McMaster-Carr, "Stainless Steel Tubing," [Online]. Available: http://www.mcmaster.com/#standard-stainless-steel-hollow-tubing. [Accessed 26 June 2012].

[65] M. J. Manahan, C. N. McCowan and M. P. S. Manahan, "Percent Shear Area

Determination in Charpy Impact Testing," *Journal of ASTM International,* pp. 1-28, 2008.

[66] M. M. Yovanovich, "Micro and Macro Hardness Measurements, Correlations, and Contact Models," *44th AIAA Aerospace Sciences Meeting and Exhibit,* pp. 1-28, 2006.

[67] Gunnar Ryge and G. Lysell, "Micro-Indentation Hardness," *Journal of Dental Research,* vol. 40, no. 6, pp. 116-1126, 1961.

[68] ASTM D790 Testing Equipment, "3 Point Flexural Bend of Plastics and Composites," [Online]. Available: http://www.testresources.net/by-test-application/flexural-bend-testing-equipment/3-point-flexural-bend-plastics-composites-astm-d638-machines/>. [Accessed 30 Aug 2012].

[69] E. P. Popov, Engineering Mechanics of Solids, New Jersey: Prentice Hall Upper Saddle River, 1998.

[70] Roy R. Craig Jr., Mechanics of Materials, 3rd ed., Wiley, 2011.

[71] B. Wielage and A. Dorner, "Corrosion Studies on Aluminium Reinforced with Uncoated and Coated Carbon Fibers," *Composites Science and Technology,* vol. 59, pp. 1239-1245, 1999.

[72] D. D. Chung, Carbon Fiber Composites, Washigton: Butterworth-Heinemann, 1994.

[73] S. Bao, K. Tang and A. Kvithyld *et al.*, "Wetting of Pure Aluminium on Graphite, SiC and Al2O3 in Aluminium Filtration," *Science Press,* vol. 22, pp. 1930-1938, 2012.

[74] D. R. Humbert, *Thesis: Modeling of Resin Transfer Molding of Composite Materials with Oriented Unidirectional Plies,* Montana: Montana State University - Bozeman, 1995.

[75] V. Michaud and A. Mortensen, "Infiltration Processing of Fiber Reinforced Composites: Governing Phenomena," *Composites*, part A, no. 32, pp. 981-996, 2001.

[76] P. Mallick, Composites Engineering Handbook, New York: Marcel Dekker, Inc., 1997.

[77] R. T. Ogulata and S. Mavruz, "Investigation of Porosity and Air Permeability Values of Plain Knitted Fabrics," *Fibers and Textiles in Eastern Europe*, vol. 18, no. 5(82), pp. 71-75, 2010.

[78] V. Mahesh, P. Nair and T. Rajan *et al.*, "Processing of Surface Treated Boron Carbide Reinforced Aluminium Matrix Composites by Liquid Metal Stir Casting Technique," *Journal of Composite Materials*, vol. 45, no. 23, pp. 2371-2378, 2011.

[79] H. Okamoto, "Al-C (Aluminium-Carbon) Phase Diagram Updates," *Journal of Phase Equilibria*, vol. 13, no. 1, 1992.

[80] R. B. Silvério, R. S. Paredes and C. M. d'Oliveira, "Iron Aluminide Alloy Development using Plasma Transferred Arc Coating Process," in *COBEM: 17th International Congress of Mechanical Engineering*, 2003.

[81] E. Bayraktar and D. Katundi, "Development of a New Aluminium Matrix Composite Reinforced with Iron Oxide," *Journal of Achievements in Materials and Manufacturing Engineering*, vol. 38, no. 1, pp. 7-14, 2010.

[82] J. Davis, "Heat Resistant Materials," ASM International, 1997.

[83] K. Erhard and S. Prasan, "Chapter 3: Manufacture and Characteristics of Stainless Steel Powders," in *Powder Metallurgy Stainless Steels: Processing, Microstructures, and Properties*, ASM International, 2007.

[84] VLSI, "Diffusion and Oxidation," VLSI Research Inc., 1993.

[85] C. Tekmen and U. Cocen, "The Effect of Si and Mg on Age Hardening Behavior of Al–SiCp Composites," *Journal of Composite Materials,* vol. 37, no. 20, pp. 1791-1799, 2003.

[86] L. M. Foster, G. Long and M. S. Hunter, "Reactions Between Aluminium Oxide and Carbon," *Journal of the American Ceramic Society,* vol. 39, no. 1, pp. 1-11, 1956.

[87] H. E. Calderón, O. M. Suarez and E. Barrios, "Thermomechanical Effects on Aluminium Matrix Composites Reinforced with AlB2 Particles," *Journal of Composite Materials,* pp. 2651-2672, 2008.

[88] Torayca, "T300 Data Sheet," [Online]. Available: http://www.toraycfa.com/pdfs/T300DataSheet.pdf. [Accessed 25 March 2013].

[89] M. Pries, H. Militz and B. Goodell *et al.*, "A Note on Reinforcement of Polymer Matrix Composites Using Carbon Residues Derived from Woody Biomass," *Journal of Composite Materials*, vol. 44, no. 15, pp. 1883-1892, 2010.

[90] J. Noh and J. Whitcomb, "Effect of Transverse Matrix Cracks on the Relaxation Moduli of Linear Viscoelastic Laminates," *Journal of Composite Materials,* vol. 37, no. 6, pp. 543-558, 2003.

[91] A. Fischer-Cripps, "The Chemistry Companion," CRC Press, 2012.

[92] G. Korb, J. Korab and G. Groboth, "Thermal Expansion Behaviour of Unidirectional Carbon-Fiber-Reinforced Copper-Matrix Composites," *Osterreichisches Forschungszentrum Seibersdorf,* vol. 29, no. 98, pp. 1563-1567, 1998.

[93] G. T. Hahn and A. R. Rosenfield, "Metallurgical Factors Affecting Fracture Toughness of Aluminium Alloys," *Metallurgical Transactions,* vol. 6A, pp. 653-668, 1975.

[94] M. Nganbe, "Class Lecture," *Superalloys and Ceramic Metal Matrix Composites*, 2012.